Generalized correlations of quasiband energies in nuclei

D. Bucurescu,[1] N. V. Zamfir,[1,2,3] R. F. Casten,[2] and W. T. Chou[4]

[1]*National Institute for Physics and Nuclear Engineering, Bucharest-Măgurele, Romania*
[2]*WNSL, Yale University, New Haven, Connecticut 06520*
[3]*Clark University, Worcester, Massachusetts 01610*
[4]*National Tsing Hua University, Hsinchu 300343, Taiwan, Republic of China*
(Received 6 April 1999; published 30 August 1999)

A remarkable set of correlations of yrast and excited quasiband energies in collective nonrotor and rotor nuclei is discussed. These correlations are essentially independent of the nature of the states (e.g., yrast, quasi-γ-vibrational, superdeformed), of mass region, and of the type of nucleus (even-even, odd-A, or odd-odd), and indicate a universal behavior which apparently describes all collective low energy structures. The results also show that, for most cases in odd-A *deformed* nuclei, the band energies do *not* follow the rotational formula. The nature of spherical-deformed phase/shape transitions is also discussed and related to the seemingly (but not actually) different behavior of the neighboring even-even core nuclei. Finally, theoretical treatments that reproduce these correlations in even-even and odd-A nuclei are discussed, and new calculations with the geometric collective model are presented. [S0556-2813(99)03209-4]

PACS number(s): 21.10.Re, 21.60.Ev, 27.50.+e, 27.60.+j

I. INTRODUCTION

The properties of the lowest excited states of atomic nuclei offer a very sensitive test for nuclear structure theories. Although level energies were recognized long ago as valuable signatures of structure, their *relationships* over large nuclear regions have been rather little investigated until recently. During the last few years, however, a remarkable set of correlations has been discovered [1–7] among the excitation energies of quasiband structures in collective nuclei. These discoveries have been possible by exploiting the large body of data on stable and near-stable nuclei whose accumulation over the past decades now permits a global perspective and a synthesis of heretofore seemingly disparate behavior. The correlations found to apply to nuclei near stability offer benchmarks and challenges for confronting data soon-to-be-obtained on exotic nuclei far from stability. They also draw attention to the value of a "horizontal" approach to structural *evolution*, as a complement to the usual "vertical" approach that focuses on individual level schemes.

The first observation that triggered these investigations was that the yrast energies of the collective, nonrotational medium and heavy even-even nuclei show linear correlations [see Fig. 1(a)] which could be interpreted in the framework of an anharmonic vibrator (AHV) with a nearly *constant* anharmonicity [1,2]. Equally simple correlations have subsequently been found for precollective nuclei [3]. Similar energy correlations have also been found for quasiband structures in collective [4–6] and precollective [7] odd-A nuclei.

These findings, essentially empirical, are rather surprising. Such simple and almost universal correlations were not predicted in advance by any nuclear model and there is still no microscopic understanding of the observed behavior and
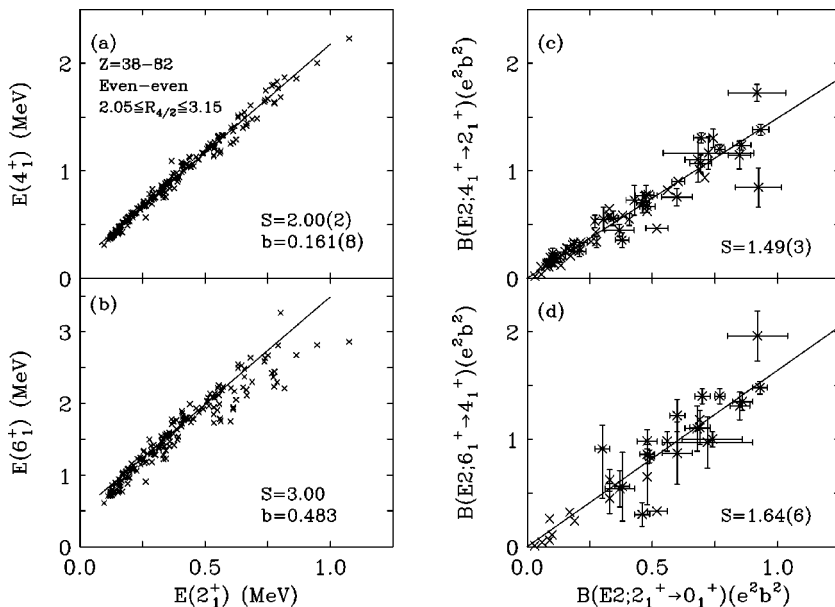

FIG. 1. Energy and $B(E2)$ correlation plots for yrast bands of the collective nonrotational even-even nuclei with $Z=38$ to 82 [1]. (a) The straight line is a fit to the data with slope $S=2.00\pm0.02$ and intercept $b=0.161\pm0.008$ MeV as indicated. (b) The straight line is the AHV prediction $E(6_1^+)=3E(2_1^+)+3\varepsilon_4$, with ε_4 taken from the fit in the upper panel. (c) Correlation of $B(E2;4_1^+\to2_1^+)$ with $B(E2;2_1^+\to0_1^+)$. (d) Correlation of $B(E2;6_1^+\to4_1^+)$ with $B(E2;2_1^+\to0_1^+)$. The data are from Ref. [8]. The straight line in (c) and (d) is a fit to the data with slope S and intercept 0.

TABLE I. Summary of the results of the observed AHV-type correlations. For each specified set of experimental data specified in the columns towards the left, the table gives the slope of the first energy correlation [Eq. (2) for $n=2$], the value ε_4, as well as the 1σ r.m.s. deviation of the experimental points from the fitted AHV line. The experimental data are from Refs. [8] and [14] (superdeformed bands). The quasiband labels for odd-A and odd-odd nuclei are inclusive; that is, the correlations include all bands of the specified type (e.g., all normal parity bands extracted from Ref. [8]) in the type of nuclei considered (e.g., nonrotational for $Z=34$–80).

Set of nuclei	Range	Quasibands	Number of cases	Slope	ε_4 (keV)	1σ-deviation (%)	Fig.nr.
			Even-even nuclei				
Nonrotational	$38 \leq Z \leq 82$	g.s.b. (yrast)	163	2.00(2)	161(8)	5.0	1
Nonrotational	$34 \leq Z \leq 82$	Quasi-γ	50	1.97(3)	104(13)	3.7	2
Nonrotational	$34 \leq Z \leq 82$	0_2^+-quasiband	57	1.86(7)	136(18)	8.0	3
			Odd-A nuclei				
Nonrotational	$34 \leq Z \leq 80$	Unique parity	329	2.01(2)	170(11)	6.4	5
Nonrotational	$34 \leq Z \leq 80$	Normal parity	276	2.02(2)	116(7)	7.4	5
Rotational	$63 \leq Z \leq 77$	Unique parity	99	2.01(2)	87(4)	3.9	6
Rotational	$63 \leq Z \leq 77$	Normal parity	200	1.99(2)	96(3)	4.6	6
			Odd-odd nuclei				
Nonrotational	$33 \leq Z \leq 79$	2-quasiparticle	305	2.05(2)	139(11)	6.0	7
Rotational	$67 \leq Z \leq 75$	2-quasiparticle	101	2.00(2)	86(6)	5.7	8
			All nuclei				
	Mass 80	SD-bands	9	2.00(1)	150(19)	2.4	17
	Mass 130	SD-bands	19	1.96(2)	98(17)	0.9	17, 18
	Mass 150	SD-bands	51	1.97(1)	71(8)	0.5	17, 19
	Mass 190	SD-bands	51	1.98(1)	47(2)	0.6	17

its universality. Nevertheless, macroscopic approaches such as the interacting boson model, as well as the interacting boson-fermion model, automatically reproduce, in a natural way, the observed behavior [2,5]. As noted already, the universality of the observed energy correlations leads to intriguing questions concerning their possible extension to the new nuclear regions that will become accessible with future studies based on radioactive beams.

The present article begins by collecting the existing scattered empirical results on these energy correlations in collective nuclei, mostly published so far in Letter form [1–7]. It then extends the study of such correlations to additional states and nuclei, such as intrinsic vibrational excitations in even-even nuclei, bands in odd-odd nuclei, and superdeformed bands. This rich experimental material points to the fact that these energy correlations are essentially similar, regardless of the nature of the states, of the mass region, of the type of nucleus, and have therefore a global, universal aspect. A simple expression is derived which economically describes the energies of any collective band. Finally, theoretical models which can reproduce such correlations are reviewed, and new results are presented for even-even nuclei with the geometric collective model.

II. GLOBAL CORRELATIONS: EMPIRICAL RESULTS

In this article we restrict ourselves to the investigation of *collective* nuclei. For even-even nuclei, a generally accepted definition is that these are nuclei with a ratio $R_{4/2} \equiv E(4_1^+)/E(2_1^+)$ larger than 2.0. For a clearer cutoff from ''precollective'' nuclei (with $R_{4/2}$ smaller than 2.0) we use the condition $R_{4/2} \geq 2.05$. During our studies it became ap-

parent that there is a natural empirical separation of collective nuclei into two subclasses: *non-rotational* nuclei ($2.05 \leq R_{4/2} < 3.15$) and *rotational* nuclei ($R_{4/2} \geq 3.15$). For odd-A and odd-odd nuclei there is no obvious single criterion to distinguish these classes of nuclei, since energy correlations depend on the spins of the levels. Hence we have investigated such nuclei according to the classification of their even-even cores. In this paper, we will discuss many ensembles of nuclei and types of states (yrast, vibrational, etc.). Table I gives a summary of, and guide to, the data shown and the results obtained.

A. Even-even nuclei

1. Yrast levels

We first present the results of Ref. [1], since this type of investigation and its results became an almost standard paradigm for the subsequent studies. The idea of Ref. [1] was very simple: instead of studying the yrast energies of even-even nuclei, $E(2_1^+), E(4_1^+), E(6_1^+), \ldots$ or their ratios, such as $R_{4/2}$, as functions of Z, A or other similar quantities, as usually done, we studied the relationships *between* the energies themselves. Figure 1(a) shows the very surprising result obtained: a plot of $E(4_1^+)$ as a function of $E(2_1^+)$, for *all* collective *nonrotational* nuclei with Z from 38 to 82, shows an unexpected linear correlation of the form

$$E(4_1^+) = 2.0 E(2_1^+) + \varepsilon_4, \quad (1)$$

where an average ε_4 is given by the intercept b. It is obvious that, for any nucleus, a value of ϵ_4 can always be obtained so that Eq. (1) is satisfied. What is surprising about the correla-

tion in Fig. 1(a) is that ϵ_4 values are nearly independent of nucleus or even mass region. For *all* collective nuclei between Sr and Pb the data are reproduced surprisingly well with a value $\varepsilon_4 = 161 \pm 8$ keV, the deviations from the linear fit of Eq. (1) being practically random, with a 1σ deviation of 5%.

The interpretation of Eq. (1) is that of an *anharmonic vibrator* (AHV) with *constant* anharmonicity [9]; the anharmonicity ε_4 is the difference between the energy of the two-phonon state $E(4_1^+)$ and twice the energy of the one-phonon state, $E(2_1^+)$. The anharmonicity can also be regarded as the phonon-phonon interaction. The constancy of ε_4 implies that, although Fig. 1 spans nuclei with a very large variety of structures [as indicated, for example, by the variation of $E(2_1^+)$] these nuclei can be considered as belonging to a single underlying class, that of an interacting multiphonon system whose phonon-phonon interaction energy manages to remain essentially constant regardless of the obvious changes that must be occuring in the internal structure of the phonon itself. An alternate way of stating this is that the structure of any of these nuclei is, to an excellent approximation, specified by the 2_1^+ energy alone.

The AHV expression of Eq. (1) can be generalized for any yrast state, as follows:

$$E(n) = nE(1) + \frac{n(n-1)}{2}\varepsilon_4. \qquad (2)$$

Here, n stands for "n-phonons." $E(n)$ is the energy of the n-phonon state, of spin $I = 2n$ and the anharmonicity is $\varepsilon_4 = E(2) - 2E(1) \equiv E(4_1^+) - 2E(2_1^+)$. For the cases discussed until now, these were the excitation energies within the yrast quasiband of even-even nuclei. We shall later apply Eq. (2) to other quasiband structures as well.

That AHV relation (1) is not an accident is supported by additional experimental data, most notably by the higher spin yrast energies using Eq. (2). Thus, for the three-phonon state (6^+), the AHV model [9] predicts an energy $E(6_1^+) = 3E(2_1^+) + 3\varepsilon_4$, where ε_4 is the same anharmonicity of the 4_1^+ state. Figure 1(b) shows that this expectation is well supported by the experimental data.

Additional evidence for this AHV description of the yrast states was discussed in Ref. [2] on the basis of the $B(E2)$ values for transitions between the states of this quasiband [e.g., the correlation of $B(E2:4_1^+ \rightarrow 2_1^+)$ with $B(E2:2_1^+ \rightarrow 0_1^+)$ values], for which the AHV model also predicts certain linear correlations. This is shown as follows. Following the approach of Refs. [9,10] we consider a system of n-phonon states, $|n\rangle$, and their creation and destruction operators $B^\dagger$ and B. The quadrupole operator corresponding to $E2$ transitions is given by

$$Q = a_1 B + a_2 B^\dagger BB + a_3 B^\dagger B^\dagger BBB + \cdots. \qquad (3)$$

The matrix element $\langle n-1|Q|n\rangle$ is then given by

$$\langle n-1|Q|n\rangle = a_1\sqrt{n}\left[1 + \frac{a_2}{a_1}(n-1) + \frac{a_3}{a_1}(n-1)(n-2)\right.$$
$$\left. + \cdots \right]. \qquad (4)$$

Since $B(E2;n \rightarrow n-1) = \langle n-1|Q|n\rangle^2$, we have $B(E2:2_1^+ \rightarrow 0_1^+) = a_1^2$ and

$$B(E2:n \rightarrow n-1) = nB(E2:2_1^+ \rightarrow 0_1^+)\left[1 + \frac{a_2}{a_1}(n-1)\right.$$
$$\left. + \frac{a_3}{a_1}(n-1)(n-2) + \cdots \right]^2, \qquad (5)$$

and, specifically

$$B(E2:4_1^+ \rightarrow 2_1^+) = 2B(E2;2_1^+ \rightarrow 0_1^+)\left[1 + \frac{a_2}{a_1}\right]^2, \qquad (6)$$

which is linear in $B(E2:2_1^+ \rightarrow 0_1^+)$.

The factor n multiplying a_1^2 [i.e., multiplying $B(E2:2_1^+ \rightarrow 0_1^+)$ value] is reminiscent of the factor n multiplying $E(1)$ in Eq. (2) but, in fact, the behavior of the $B(E2)$ expression is not at all of the same form as the AHV expression for energies. The *entire* term in brackets in Eq. (5) multiplies the $2_1^+ \rightarrow 0_1^+ B(E2)$ value and the intercept is zero. Note that truncation of Eq. (5) at the a_2 linear term gives the same results as in Ref. [9].

The data are shown in Figs. 1(c) and 1(d), for the entire range of nuclei from $Z = 38-82$.

Despite the large span of nuclei comprising many different structures from near spherical to rotational, the data cluster within a compact envelope that follows a linear trajectory against the $B(E2:2_1^+ \rightarrow 0_1^+)$ values. Of course, as in Eqs. (1) or (2), it is trivial to find coefficients a_2 such that Eq. (6) is satisfied for any given nucleus. The remarkable fact again is that a single a_2 value reproduces all the data in Figs. 1(c) and 1(d). $B(E2)$ values including higher spin yrast states are also well described by Eq. (5) including the terms in a_2 and a_3. Note that the slope in Fig. 1(c) is 1.49 which implies that $a_2 = -0.14a_1$.

There is an important point of historical interest worth making at this point, namely, that these results imply much more than the linearity of the ratio $R_{I/2}$ with $R_{4/2}$ observed in Mallmann plots [11] in which the ratio $E(6_1^+)/E(2_1^+)$ was found to be linear in $E(4_1^+)/E(2_1^+)$, and similarly for $E(I^+)/E(2_1^+)$, for $I > 6$. In fact the linearity in a Mallmann plot only demonstrates a very general energy-angular momentum relationship and says nothing about ϵ_4. To see this, we use Eq. (2) to form the Mallmann energy ratios, obtaining

$$R_{4/2} \equiv \frac{E(4_1^+)}{E(2_1^+)} = \frac{2E(2_1^+) + \varepsilon_4}{E(2_1^+)} = 2 + \frac{\varepsilon_4}{E(2_1^+)} \qquad (7)$$
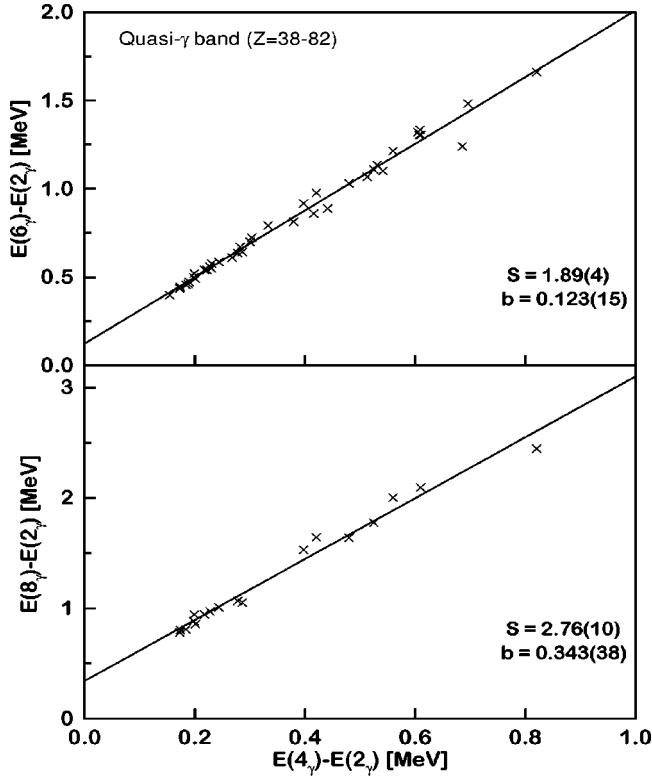
and

FIG. 2. Energy correlation plots similar to those of Fig. 1, but for the quasi-γ bands of the collective, nonrotational nuclei with Z between 34 and 82. The straight lines are fits to the data, with the slope S and intercept b as indicated. Data from Ref. [8].

$$R_{6/2} \equiv \frac{E(6_1^+)}{E(2_1^+)} = \frac{3E(2_1^+) + 3\varepsilon_4}{E(2_1^+)} = 3 + 3\frac{\varepsilon_4}{E(2_1^+)}, \quad (8)$$

and hence

$$R_{6/2} = 3R_{4/2} - 3. \quad (9)$$

From this equation we see that the Mallmann expression effectively eliminates ε_4: two nuclei with ε_4 values orders of magnitude apart would still lie on a linear Mallmann trajectory. Indeed, the linear trajectory of a Mallmann plot automatically results from *any* two-parameter energy-angular momentum relation. Moreover, even the specific linear trend seen in the empirical Mallmann plot $R_{6/2}$ namely $R_{6/2} \sim 3R_{4/2} - 3$, only implies that $E(I)$ is proportional to I and/or I^2: it says nothing further, nor does it imply a constancy of ε_4 (or of b in the Ejiri relation [12]).

2. Intrinsic excitations

The simple method applied above to the yrast states, of examining correlations between excitation energies within a certain quasiband, can be applied to quasibands based on intrinsic excitations [13]. Figure 2 shows the results for the quasi-γ band; here, the zero-phonon (or the reference) state is the 2_γ^+ state and the other states are those of the $\Delta I = 2$ sequence $(4^+, 6^+, \dots)$ built above it. One can see that the
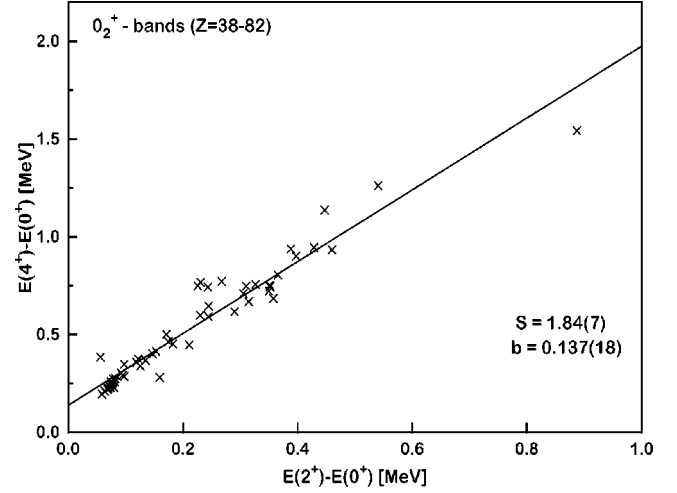

FIG. 3. Same as Fig. 2, for 0_2^+-bands in the nuclei with $Z = 34$ to 82.

empirical correlation is well described by Eq. (2) with an ε_4 value somewhat smaller than that for the yrast states (about 100 keV).

Similarly, Fig. 3 shows the same type of correlation for the bands built on the lowest 0^+ state intrinsic excitation (the 0_2^+ state). Although a large ensemble of nuclei has been chosen, and the nature of the different 0_2^+ states certainly differs, there is still a rather good linear correlation, with only slightly more scatter of the points than for the yrast levels. The correlation is close to Eq. (1) with a value ε_4 similar to that for the yrast states. Thus, it appears that the correlations observed for the yrast states characterize excited modes as well.

Finally, we examine *rotational* even-even nuclei. In these nuclei, the energies must be close to the formula $E_{rot}(4_1^+) = 3.33E(2_1^+)$. This can be obtained from the AHV formula, Eq. (1), provided ε_4 is taken as $\frac{4}{3}E(2_1^+)$, that is, $E_{rot}(4_1^+) = 2E(2_1^+) + \frac{4}{3}E(2_1^+)$. But, in this case ε_4 will, of course, not be constant. Indeed, since the rotational formula gives $E(2_1^+) = 6(\hbar^2/2\mathcal{I})$ we have $\varepsilon_4 = 8(\hbar^2/2\mathcal{I})$ which should vary as the rotational constant $\hbar^2/2\mathcal{I}$. The results are shown in Fig. 4 for the nuclei in the deformed rare earth region with $A \sim 150-190$ and $R_{4/2} > 3.24$. The upper section shows that these data lie along a line of slope 3.33. The lower section extracts the resulting ε_4 values and confirms that they indeed vary linearly with $E(2_1^+)$. This behavior, of course, is expected. We highlight it here because we will see below that the data for odd-A deformed nuclei contrast markedly.

B. Odd-A nuclei

We now examine energy relationships within the lowest $\Delta I = 2$ quasiband structures of odd-A nuclei (one-quasiparticle structures). From now on, the states ''n'' in the sense of Eq. (2) are those of spin $I = J + 2n$ of a given quasiband; usually J is the spin of the ''bandhead,'' but, in principle, as will be discussed below, one can use another state of the band as a ''basis.'' These considerations are also valid for odd-odd nuclei.
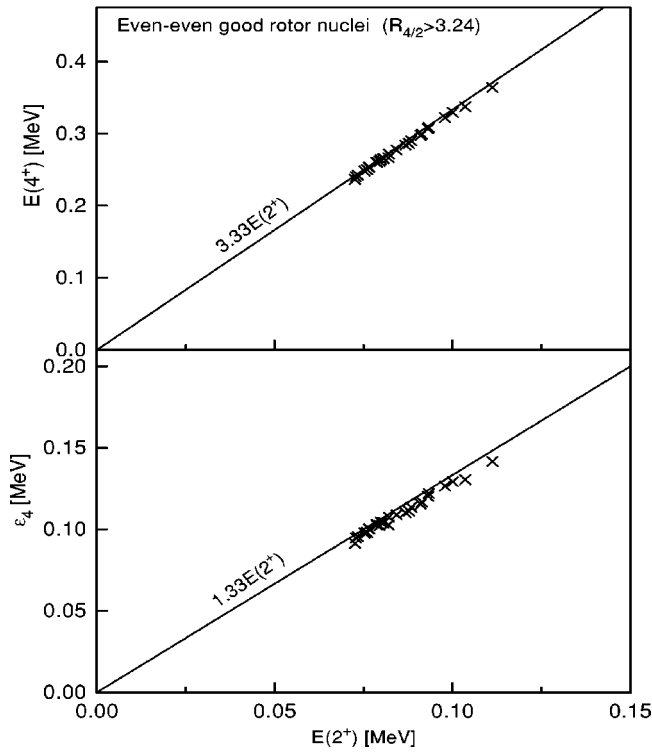
FIG. 4. Energy correlation plots for the yrast bands of good rotor even-even nuclei ($R_{4/2}>3.24$). The solid lines show the behavior expected in the rotational limit (in this case, the ε_4-value of Eq. (1) is $\frac{4}{3}E(2_1^+)$).

1. Nonrotational nuclei

Even knowing the results for even-even nuclei (that is, the universality of the AHV correlation), it is difficult to make a prediction of what is expected to happen for odd-mass nuclei. As is well known, the characteristics of the structures resulting from coupling a particle to an even-even core depend on many factors, important among which are the deformation, the Fermi level, the single particle orbitals available, Coriolis mixing, etc., and how each of these varies with Z and N. There are quite a few limiting ''coupling'' schemes recognized: in some of them the quasiband structures bear resemblance to the yrast band of the core structure, while in others they are quite different.

The first empirical study considered only the quasibands based on the unique parity orbitals (UPO) [4]. This case was studied first because it was considered more transparent, since such orbitals have practically no mixing with other orbitals. For each UPO, of spin j, the spin sequences considered were the ''favored'' quasiband ($J=j$), and, separately, when available, the ''unfavored'' quasiband ($J=j-1$), even if in some cases the respective structures started at spins lower than j. It was shown that for nonrotational nuclei with Z between 34 and 78 both sequences of states obeyed rather nicely the AHV formula (2), with an ε_4 value close to that of the yrast states in the even-even nuclei. In this paper we relax the condition that for each UPO one starts always from the state of spin j and consider now states from the lowest one known. The only (rare) exception is when the state of lowest

spin of the structure is not also lowest in energy—in this case one starts from the lowest state in energy. The same approach is used for the bands based on normal parity orbitals, considered for the first time in Ref. [5].

The empirical results are displayed in Fig. 5, where all odd-A nuclei between Ge and Hg were taken into consideration. The correlation is very similar to that in Fig. 1, the AHV relation (2) describing very well the average behavior of this rather large collection of data. The scatter of the points may be somewhat larger than that in Fig. 1; on the other hand, one should emphasize that practically all known band structures in the nuclei with Z between 34 and 80 [8] are represented in Fig. 5. Regional systematics present less scatter.

2. Rotational nuclei

Band structures in rotational odd-A nuclei were considered in Ref. [6]. These results are presented in Fig. 6 in a slightly different form (separately for UPO and normal parity orbital bands). The data again show extremely well-correlated patterns, described by the same formula, Eq. (2), with constant ε_4, even though these nuclei are rotational. This behavior is qualitatively different than for even-even nuclei (Fig. 4). This apparent paradox and its implications will be discussed in the next section.

C. Odd-odd nuclei

The same type of energy correlations were investigated for a collection of quasibands in odd-odd nuclei with Z between 33 and 79 (the lowest two-quasiparticle bands in these nuclei). Figures 7 and 8 show the lowest two energy correlations in these bands, separately for the nonrotational and rotational nuclei, respectively. All these correlations are again found in good agreement with the AHV formula (2), with ε_4 values comparable to those found for even-even or odd-A nuclei (see also Table I).

III. DISCUSSION

A. Odd-A nuclei

To this point, we have mostly presented empirical energy correlations for quasiband structures at low excitation energy in all nuclei with Z between 34 (mass ~70) and 80 (mass ~200). While the results shown in Figs. 1, 4, 5 and 6 were already known, those in Figs. 2 and 3 (concerning intrinsic excitations in even-even nuclei) and in Figs. 7 and 8 (for odd-odd nuclei) are essentially new. Inspection of Figs. 1 to 8, as well as of Table I, shows that the AHV-type of correlation—Eq. (2)—is well obeyed by practically all quasiband structures considered in all collective medium-heavy nuclei. From Table I one sees that the ε_4 value may vary somewhat with the mass range, the type of quasiband, or with the class of nuclei (rotational or nonrotational). Still, the remarkable result is that for large sets of nuclei/quasibands, including up to hundreds of cases, an AHV behavior (2) with *constant* ε_4 is observed. The only exception is rotational bands in even-even nuclei where $E=(\hbar^2/2\mathcal{I})I(I+1)$ implies that ε_4 varies linearly with $E(2_1^+)$. In odd-A and odd-
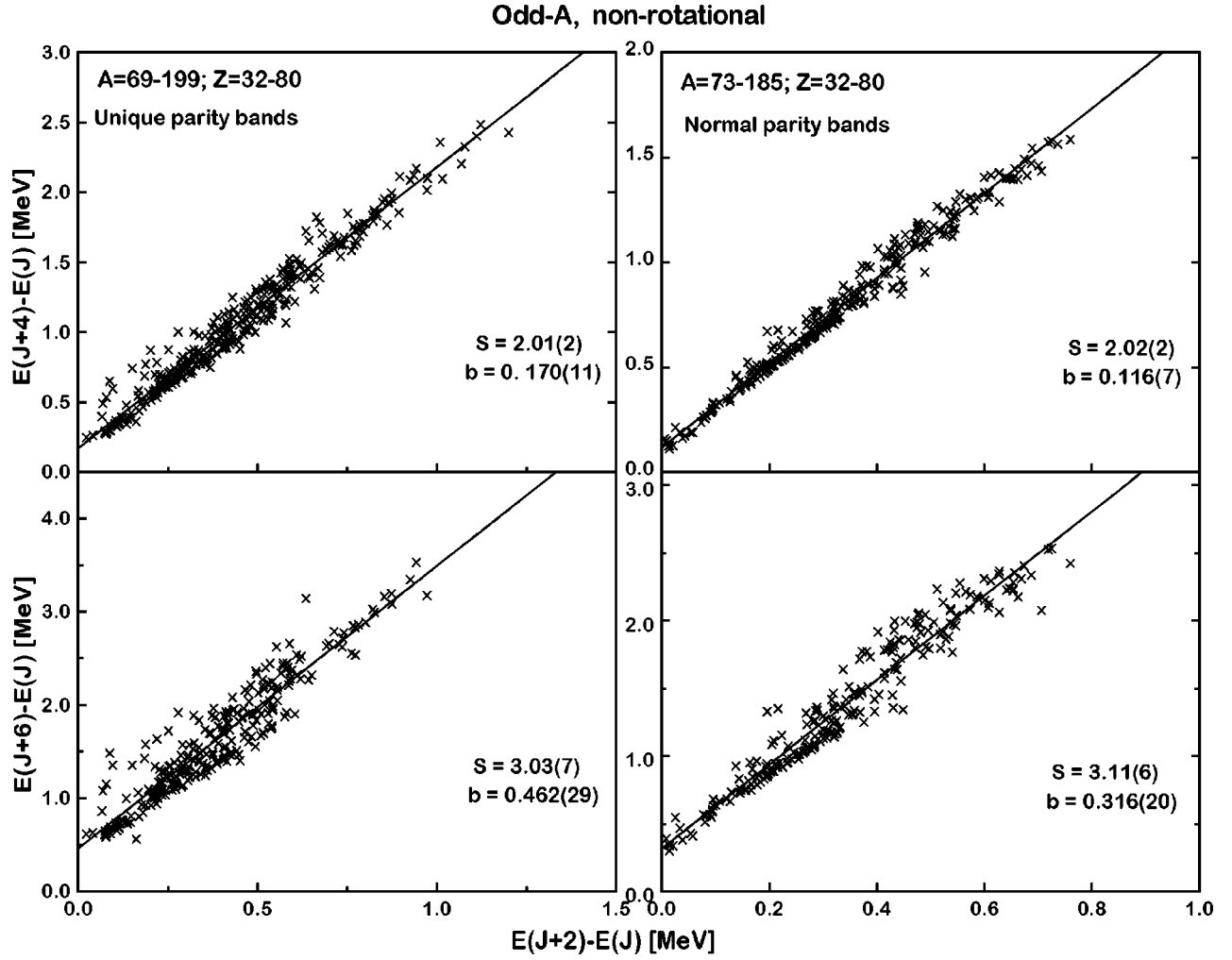
FIG. 5. Energy correlation plots for one-qp quasiband structures in odd-*A* nonrotational nuclei with *Z* from 34 to 80, for unique parity (left) and normal parity (right) orbitals, respectively. The curves are straight line fits to the data, with slope *S* and intercept *b* as indicated. The relation with Eq. (2) is through the notation $E(n) = E(J+2n) - E(J)$.

odd nuclei, ε_4 is constant *even* for rotational nuclei. However, the *meaning* of the observed correlations is different for the nonrotational and rotational nuclei, respectively.

The rotational formulas that successfully describe many bands in rotational nuclei are well known and it is therefore worthwhile to investigate under which circumstances they may be compatible with AHV-type correlations. To be more specific, we consider the strong coupling formula for odd-*A* nuclei, for which the band energies as a function of spin read (neglecting the Coriolis interaction)

$$E(I) = \frac{\hbar^2}{2\mathcal{I}}[I(I+1) - K(K+1)]. \tag{10}$$

Let us choose as reference a state of spin *J* from the band and define excitation energies in the band with respect to this state:

$$E(1) = E(J+2) - E(J) = \frac{\hbar^2}{2\mathcal{I}}(4J+6),$$

$$E(2) = E(J+4) - E(J) = \frac{\hbar^2}{2\mathcal{I}}(8J+20), \quad \dots,$$

$$E(n) = E(J+2n) - E(J) = \frac{\hbar^2}{2\mathcal{I}}[4nJ + 2n(2n+1)]. \tag{11}$$

Assuming now that the moment of inertia $\mathcal{I}$ is *constant* we can rewrite Eqs. (11) in two distinct ways as

$$E(n) = \frac{2nJ + n(2n+1)}{2J+3} E(1), \tag{12}$$

or

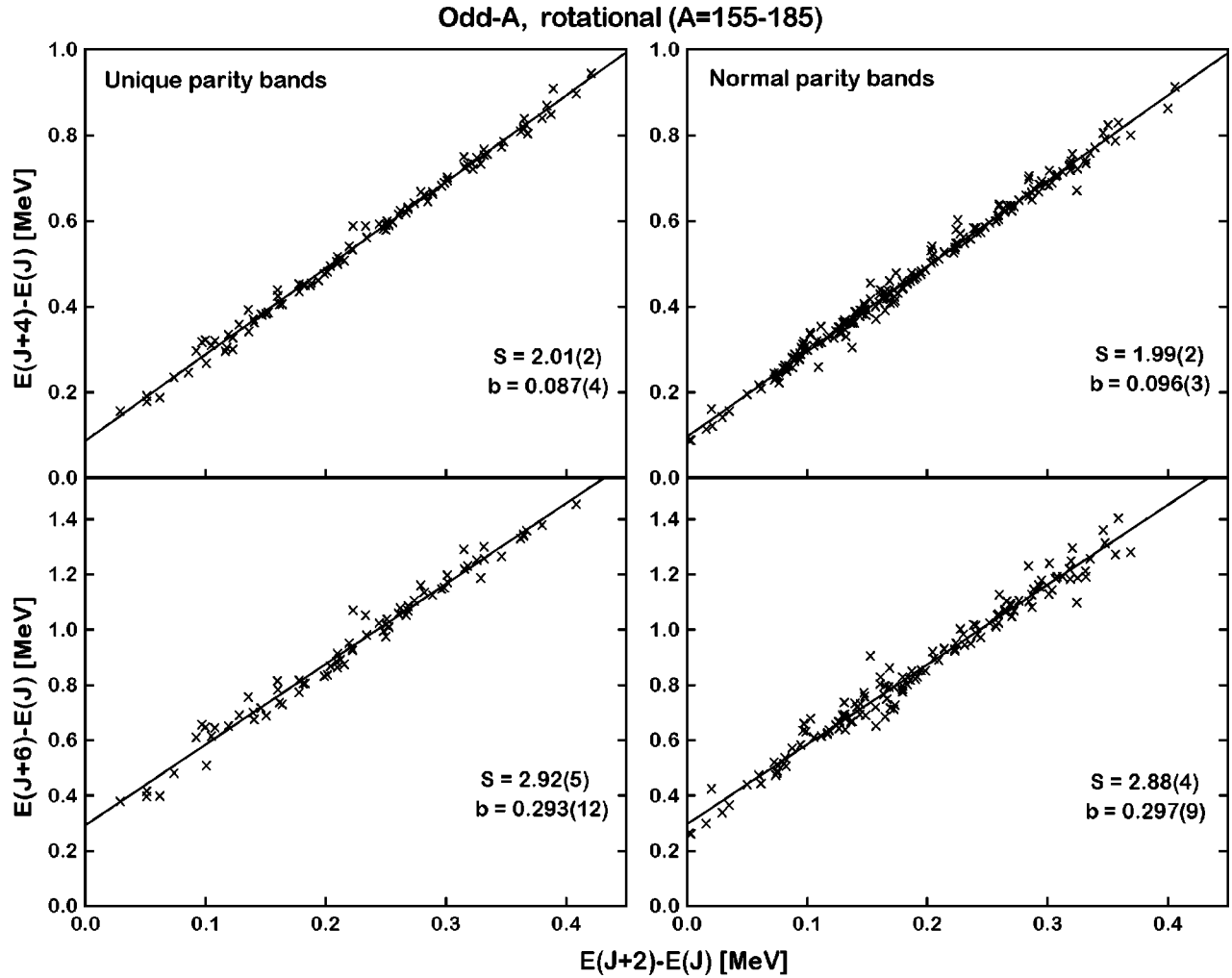$$E(n) = nE(1) + \frac{n(n-1)}{2} \varepsilon_4, \tag{13}$$

where

FIG. 6. Same as Fig. 5, for bands in odd-*A* rotational nuclei.

$$\varepsilon_4 = 8\frac{\hbar^2}{2\mathcal{I}}. \tag{14}$$

Equations (12) and (13) present an apparent paradox. We first note that Eq. (13) is formally identical with Eq. (2); thus, for $n=2$, $E(2)$ is linear in $E(1)$ with slope 2.0 and *finite* intercept ε_4. However, Eq. (12) states that $E(2)$ is linear in $E(1)$ with slope $(4J+10)/(2J+3)$ with *zero* intercept. How does one understand this seemingly contradictory behavior when both formulas result directly from Eqs. (11)? This situation is schematically illustrated in Fig. 9.

Assuming constant moment of inertia, the only way formulas (12) and (13) with constant ε_4 can be simultaneously satisfied is if the points for each *J* value are clustered at a single abscissa value. As indicated by open circles in Fig. 9 each of these clusters *must* be on the line from Eq. (12) corresponding to that *J* and, taken together, they must follow Eq. (13). Then, trivially, Eq. (12) is satisfied for each *J*: the points for a given *J* are all degenerate. Equation (13) is satisfied by connecting the points of different *J*. Of course, the rotational data points could lie *along* each of the trajectories of Eq. (12), with different slopes for each *J*. Then, Eq. (13) can still be satisfied but only with a variable ε_4, i.e., a chang-

ing moment of inertia, as in the case for even-even nuclei (see Fig. 4). We have already seen, though, that this is *not* the case experimentally—the data follow Eq. (13) for $n=2$ exactly with slope 2.0 and finite intercept ε_4.

Hence we are left with the only apparent explanation being one in terms of a clustering of points. To test this, we show again the data of Fig. 6, top, but with the rotational expressions of Eqs. (12) and (13) superposed. Figure 10 shows the unique parity data, Fig. 11 the normal parity data. Careful inspection of these figures shows that there is no clustering. The data for each *J* in Figs. 10, 11 are *not* clustered at a given point along the horizontal axis but span linear segments which do *not* show the behavior of Eq. (12). We can see this more clearly by showing the same data separately for each *J* value. This is done in Figs. 12 and 13. Figure 12 shows that, whenever the curves from Eqs. (12) and (13) differ significantly, and enough data is available, the data follows the AHV line with *constant* ε_4 given by Eq. (13) and not Eq. (12). The same is true for the normal parity orbits, Fig. 13, although to a slightly lesser degree.

These results are surprising. We might have expected Eq. (12) to be satisfied and that the application of Eq. (13) should have required varying ε_4 values to match varying moments
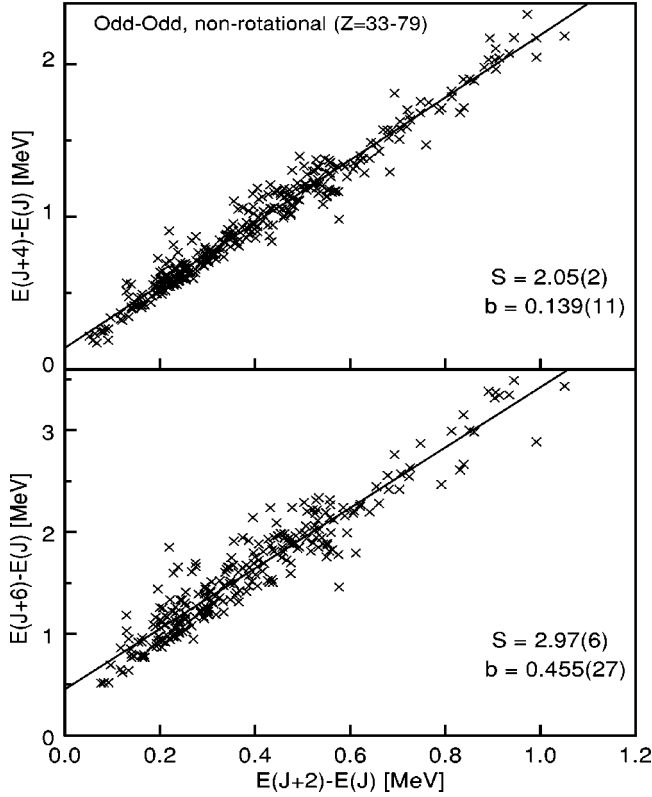
FIG. 7. Energy correlation plots for two-quasiparticle quasiband structures in nonrotational odd-odd nuclei, with $Z=33$ to 79. The curves are straight line fits to the data, of slope S and intercept b as indicated.

of inertia. In fact, however, the opposite occurs. These *rotational bands* follow the constant anharmonicity AHV formula with slope 2.0, instead of the rotational formula with slope ranging from 3.0 for $J=1/2$ and reaching 2.0 for very high J.

A general explanation for this unexpected behavior is not clear. However, for certain bands it can be understood as a consequence of the Coriolis effect.

The data points for $J=1/2$ and $J=5/2$ in Fig. 13, with low $E(1)$ values (below about 100 keV) all come from bands built on the proton Nilsson orbital [541]1/2 which is strongly Coriolis perturbed [8]. For $K=1/2$ bands the Coriolis mixing modifies the rotational energy formula of Eq. (10) so that it takes the form

$$E(I)=\frac{\hbar^2}{2\mathcal{I}}\left[I(I+1)+a(-)^{I+1/2}\left(I+\frac{1}{2}\right)\right], \qquad (15)$$

where a is the decoupling parameter. Following the same procedure as above, one can easily calculate the energies $E(n)$ for the sequence of states of spins $(J+2n)$ ($n=0,1,2,\ldots$). Thus, for the sequence of spins $1/2,5/2,9/2,\ldots$ the phase factor $(-)^{I+1/2}$ is -1 and the analogue of formula (12) is

$$E(n)=\frac{2nJ+n(2n+1)-na}{(2J+3)-a}E(1). \qquad (16)$$

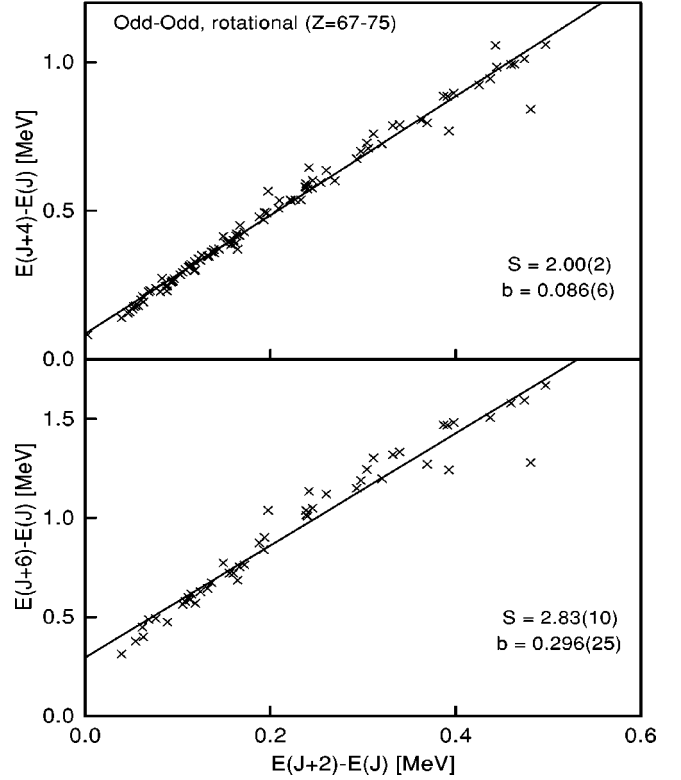

FIG. 8. Same as Fig. 7, for bands in rotational odd-odd nuclei (Z from 67 to 75).

Formula (13) does not change and ε_4 continues to have the same value as in Eq. (14).

Equation (16) is shown in Fig. 14 for several a values in comparison to Eq. (13). For $K=1/2$ bands the effect of the Coriolis mixing is to shift the points *along* the AHV line of Eq. (13): their deviations from the unperturbed position [$a=0$ in Eq. (16)] depending on the value of a. This nicely
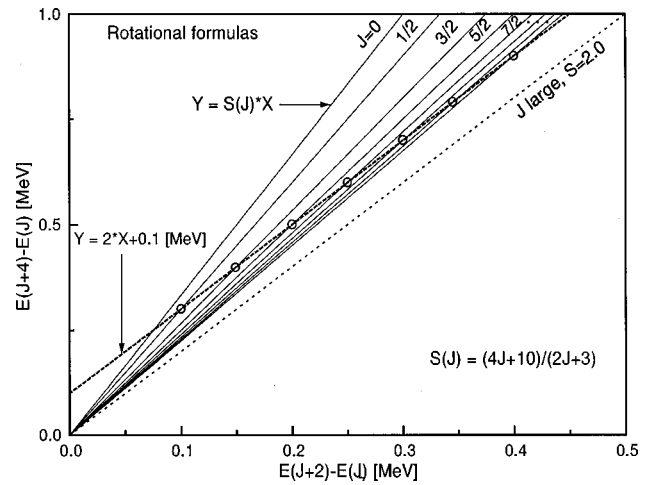

FIG. 9. Schematic illustration of the rotational energy formulas described by Eqs. (12) and (13) for $n=2$; for easy comparison with real data, an $\varepsilon_4=0.1$ MeV value has been chosen. The circles represent the intersection of the family of lines described by Eq. (12) with the AHV line [Eq. (13)].
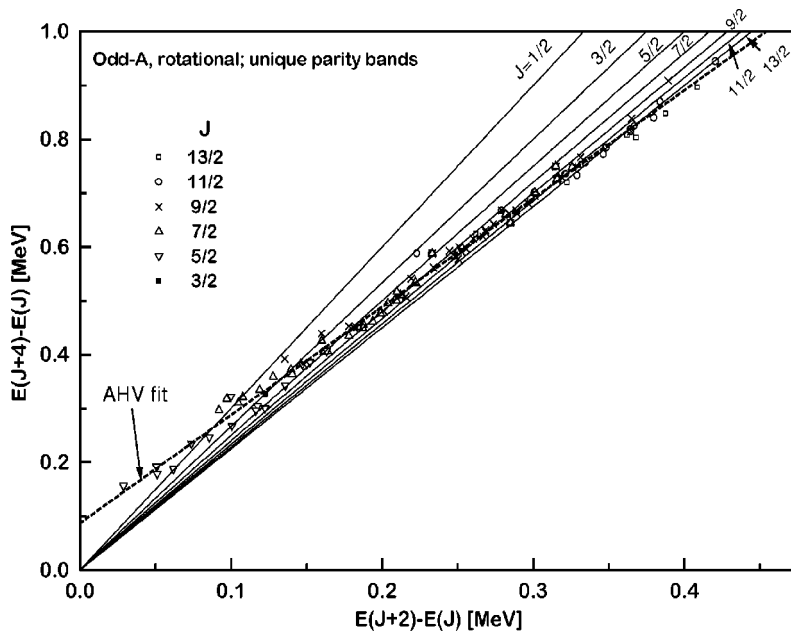
FIG. 10. The same data of Fig. 6, for unique parity bands in rotational odd-*A* nuclei, but plotted with a different symbol for each *J*-value, where *J* is the spin of the first state in the band. The family of curves described by Eq. (12), and the global AHV fit with Eq. (13) for $n=2$ are also indicated.

explains the points with low $E(1)$ and $J=1/2$ and 5/2 from Fig. 13. Indeed, the six $J=1/2$ points with $E(1)<50$ keV are [541]1/2 bands in ^{171}Lu, ^{169,167}Tm, and ^{165,163,161}Ho, and have large decoupling parameters, between about 4.0 and 2.3 [8]. Similarly, the first five points with $J=5/2$ and $E(1)$ <100 keV are [541]1/2 bands in ^{183}Re, ^{177,175}Lu, and ^{177,175}Ta, and have also large decoupling parameters (e.g., 7.5 in ^{183}Re, 5.4 in ^{177}Ta, and 4.2 in ^{173}Lu). Thus, for $K=1/2$ bands, there is in fact no contradiction between Eq. (16) and Eq. (13). This applies to the data points for $J=1/2$ and 5/2. All these points, with the exception of that of ^{183}Re, are situated on an AHV line of slope 2.0 and intercept $\sim$86 keV (slightly smaller than that of 96 keV given by the global fit in Fig. 6).

The generalization of Eq. (12) that is given in Eq. (16) actually provides a means of extracting the value of the de-

coupling parameter *a*. This may seem a tedious way to extract a quantity that has been extracted for decades from the lowest three spin members of $K=1/2$ rotational bands. However, we note that the present method uses *only* the favored or the unfavored states, not both. The advantage of this is that often in heavy ion induced reactions, the flow of γ-ray decay passes predominantly through one of these sequences (usually the favored). Where both methods of extracting *a* values are available, those deduced by intersecting Eq. (13) with the lines of Eq. (16) are in good agreement with those obtained from a fit of Eq. (15) to successive band energies [8]. An interesting observation is that even for strongly perturbed $K=1/2$ bands the AHV line (13) still provides the *correct* moment of inertia of the band [via Eq. (14)].

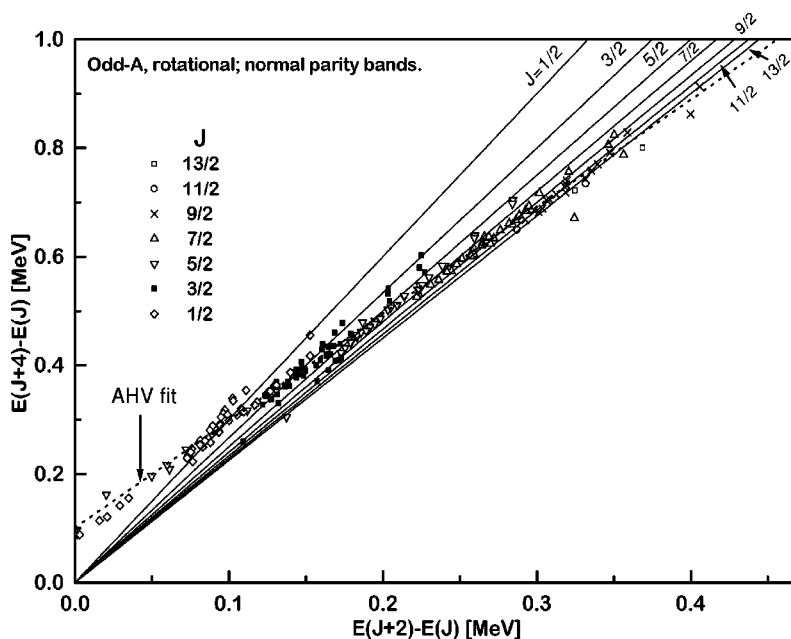For $K\neq 1/2$ bands it is impossible to estimate the general
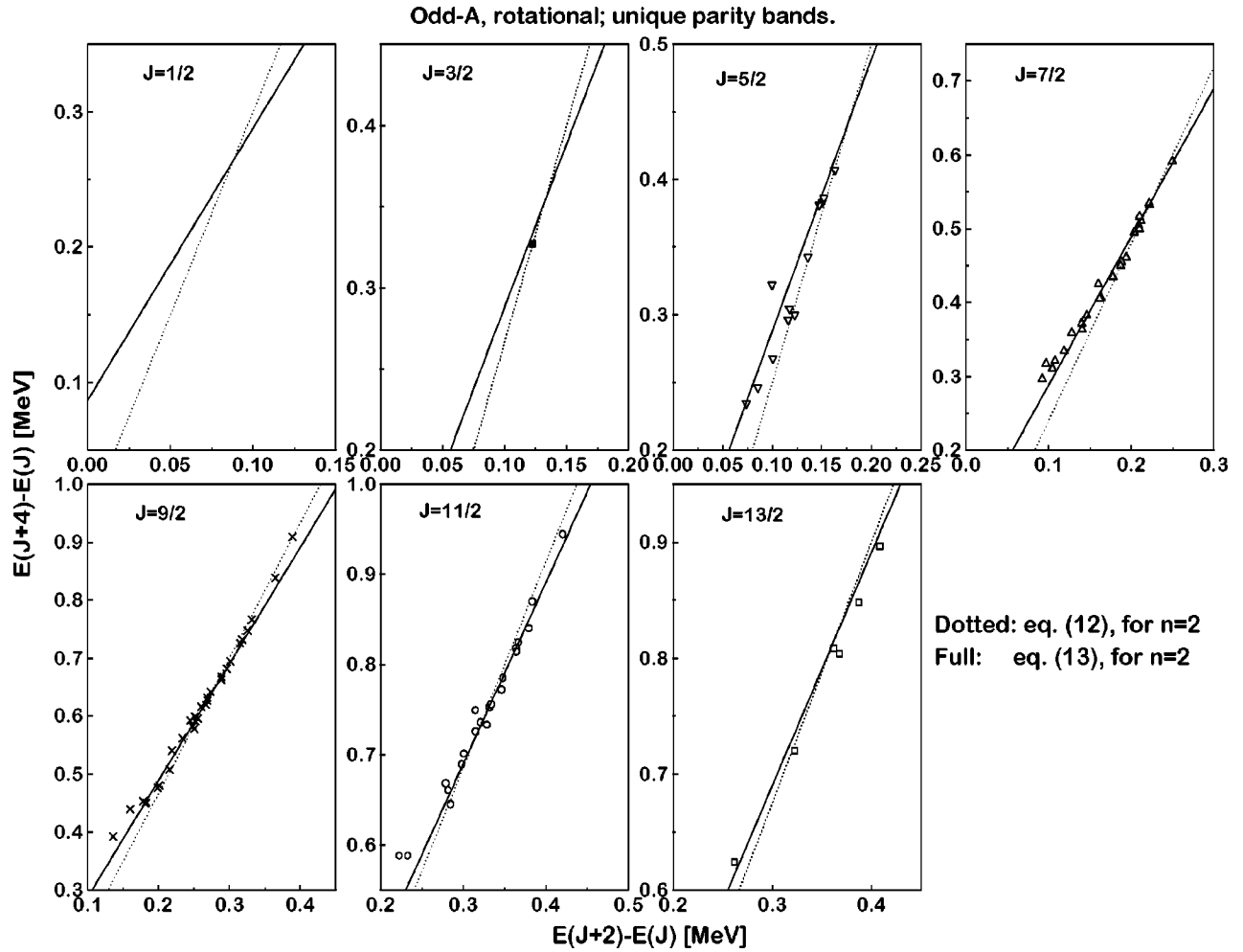

FIG. 11. Same as Fig. 10, for normal parity bands.

FIG. 12. Similar to Fig. 10, but decomposed according to the individual *J*-value (the spin of the ''bandhead''). In each panel the experimental points are shown and the line described by Eq. (12) for the given *J*, as well as the line representing the global AHV fit, with Eq. (13), to all data.

effect of the Coriolis interaction in a simple way. They will vary with nucleus, band, and mass region and therefore we are left with the paradoxical situation that the $K \neq 1/2$ ''rotational'' bands of deformed odd-*A* nuclei satisfy the AHV formula of Eq. (13) better than the rotational formula of Eq. (12).

Although we do not understand why this occurs what remains striking in the plots of Fig. 6 is the extraordinary compactness of the correlation patterns around the AHV lines. Although we do not fully understand why this is so, it looks fair to characterize this situation by the fact that the moments of inertia of all these nuclei (in the lowest part of the bands) are clustered rather around the value given by the well defined intercept of the AHV line. This ''constant'' moment of inertia behavior contrasts with the common perception that the moment of inertia varies continuously with mass, approximately as $A^{5/3}$. But there seems to be a mechanism which ''compensates'' this variation. Thus, in Fig. 15 we represent all bands in rotational nuclei (the data of Fig. 6), but now labeled according to two classes: ''lighter mass'' ($A = 155-169$) and ''heavier mass'' ($A = 171-187$). According to the $A^{5/3}$ dependence of $\mathcal{I}$, we would expect that the

symbols representing the ''heavier mass'' nuclei would be situated generally *below* those of the ''lighter mass'' group (by $\sim 15-20\%$), but, on the contrary, they come, in average, slightly higher in the plot. Figure 16 shows the same effect from a different perspective. The figure gives the distributions of the moments of inertia themselves, as deduced from the value of the first energy in the band: $\mathcal{I}/\hbar^2 = (2J+3)/E(1)$. Again, the distributions for the ''heavier mass'' nuclei are centered on lower values than those of the ''lighter mass'' nuclei. An interesting observation is also that the average ''constant'' $\mathcal{I}$ value of about $40\hbar^2$ MeV^{-1} which results from both the ε_4 values (Table I), or from the distributions of Fig. 16, is comparable with the maximum moment of inertia reached by the even-even rotational nuclei in their 2_1^+ state [corresponding to $E(1) \approx 70$ keV]. A possible explanation of the effect observed in Figs. 15 and 16 might be that the increase of the moment of inertia from the light rare earths ($Z < 70$) to the heavier nuclei ($Z > 70$) expected from the $A^{5/3}$ dependence is compensated by the larger deformations encountered in the former nuclei. It would be interesting to study the phenomenon in Figs. 15 and 16 in light of
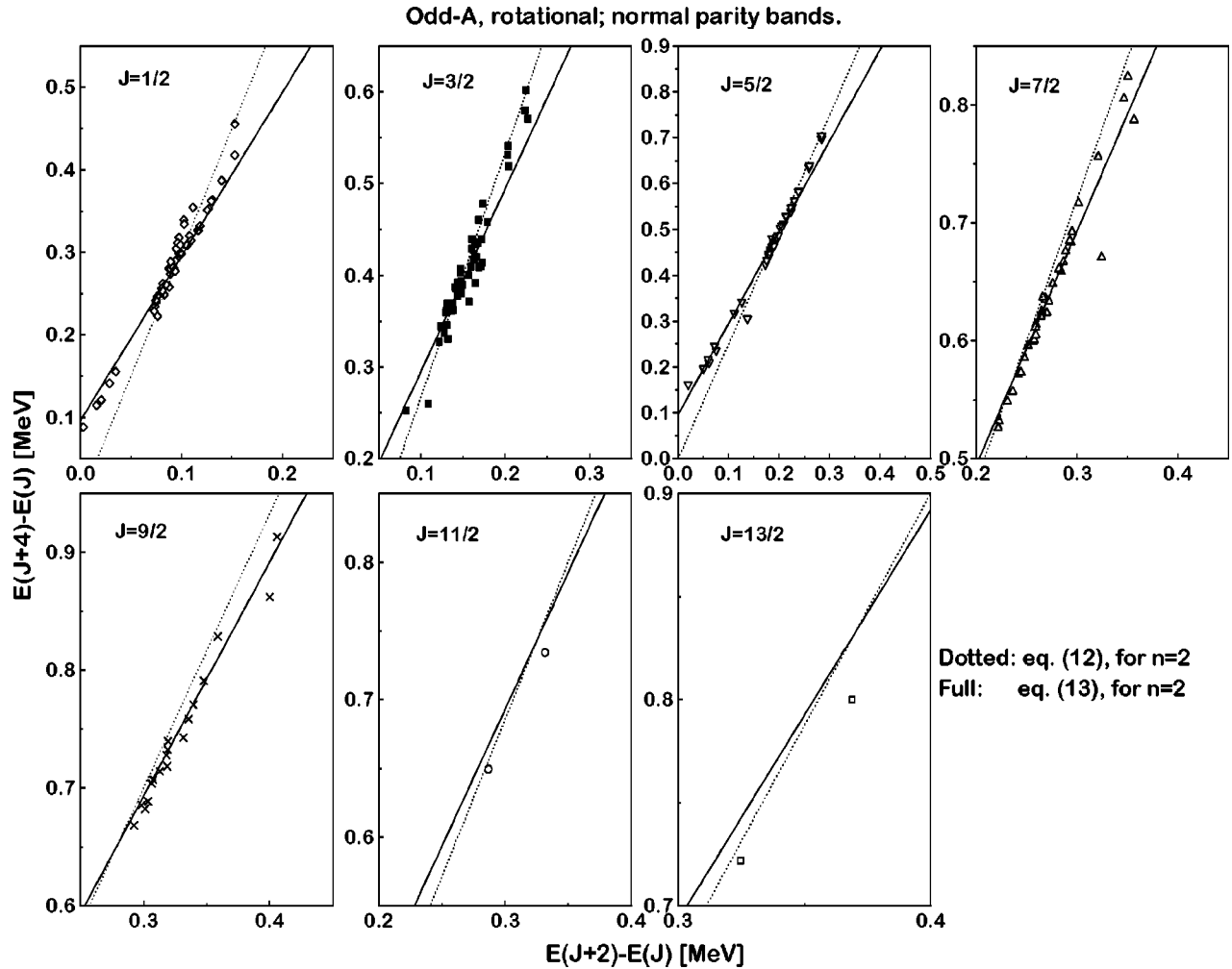
Odd-A, rotational; normal parity bands.

FIG. 13. Same as Fig. 12, for normal parity bands (data identical with those of Fig. 11).

the identical band phenomenon which has been identified *both* at high and low spin.

We now turn to perhaps the most dramatic and pure of all rotational bands, namely, superdeformed (SD) bands. Figure 17 shows the lowest correlations (for $n=2$) between energies in these bands. SD bands have been found now in at least four mass regions: ~ 80, ~ 130, ~ 150, and ~ 190 [14]. Figure 17 shows that for each of these regions there is a
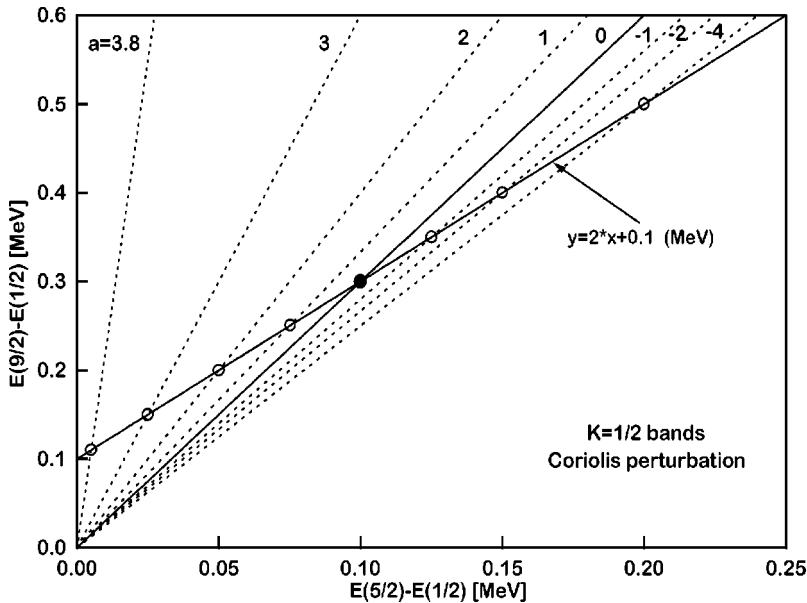

FIG. 14. Schematic illustration of the effect of the Coriolis mixing for the $K=1/2$ bands. The full line is the "AHV" line (13), and the dotted lines are representations of Eq. (16) with $n=2$ for different values of the decoupling parameter a, as indicated. The open circles show the positions where data are expected [for a given moment of inertia, here corresponding to $\varepsilon_4=0.1$ MeV—see Eq. (14)] for different a-values, whereas the black circle shows the unperturbed position (for $a=0$).
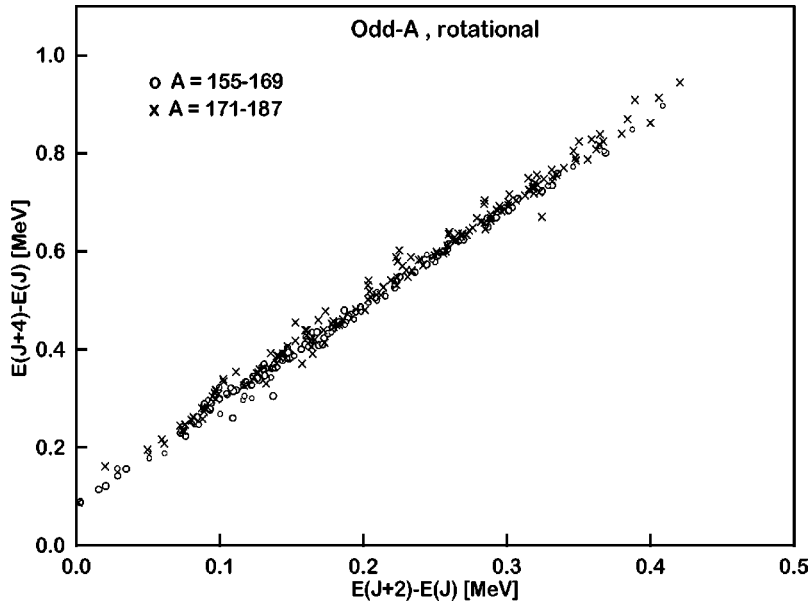
FIG. 15. Energy correlation plot for odd-*A* rotational nuclei; this plot corresponds to *all* data from Fig. 6. The two symbols correspond to nuclei with lower masses (155 to 169)—circles, and higher masses (171 to 187)—crosses.

rather well defined correlation of the form of Eq. (13). The different intercept values (see also Table I) reflect the average value of the moment of inertia of the SD bands for each mass region at the beginning of the band.

Figure 18 illustrates the in-band correlations for the first few states in the SD bands from the mass region $A \approx 130$.
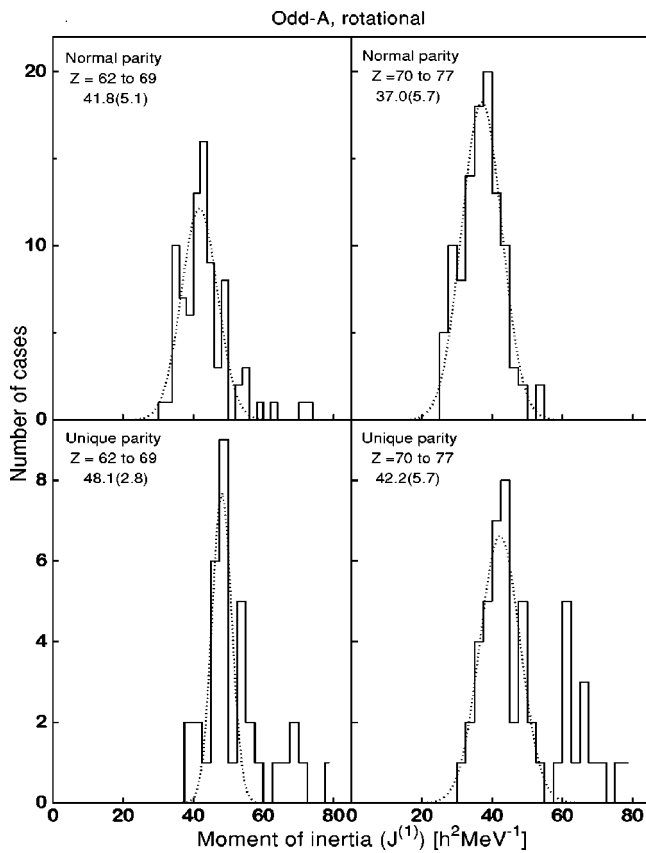

FIG. 16. Distributions of the moments of inertia of the different rotational bands represented in Figs. 6 and 15, as deduced from the first transition energy in the band according to formula (4). The few points representing the $K = 1/2$ bands with strong Coriolis perturbations discussed in Sec. III B [with $E(1) < 0.1$ MeV] are the only ones not shown in these plots. Gaussian fits (dotted lines) to the distributions plotted give the indicated mean values and 1σ deviations (in units of $\hbar^2$ MeV^{-1}).
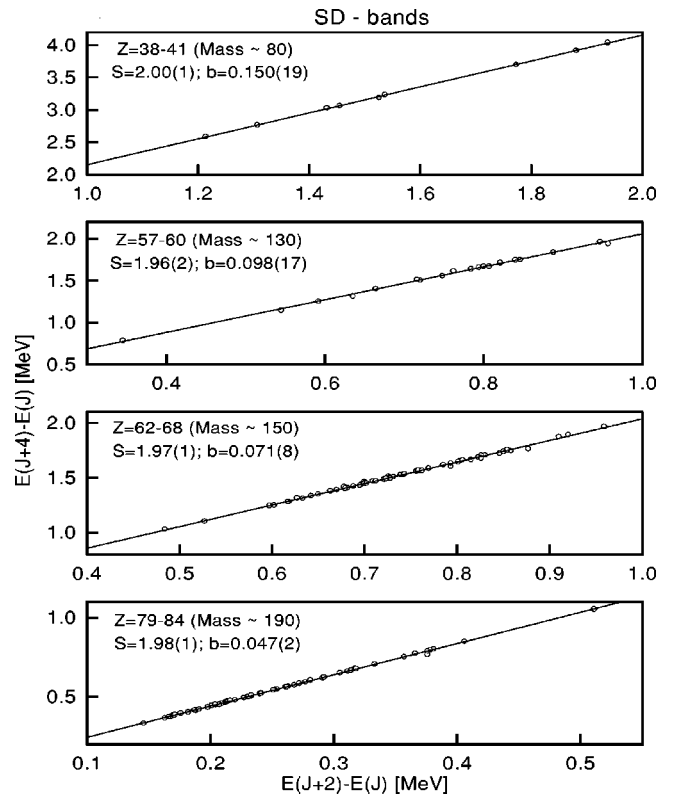

FIG. 17. Straight line fits—with Eq. (13)—to energy correlation plots for superdeformed bands in the four indicated mass regions. The resulting slopes S and intercepts *b* are indicated. The data are from Ref. [14], and for each band one starts from the lowest state known (of spin *J* usually unknown).
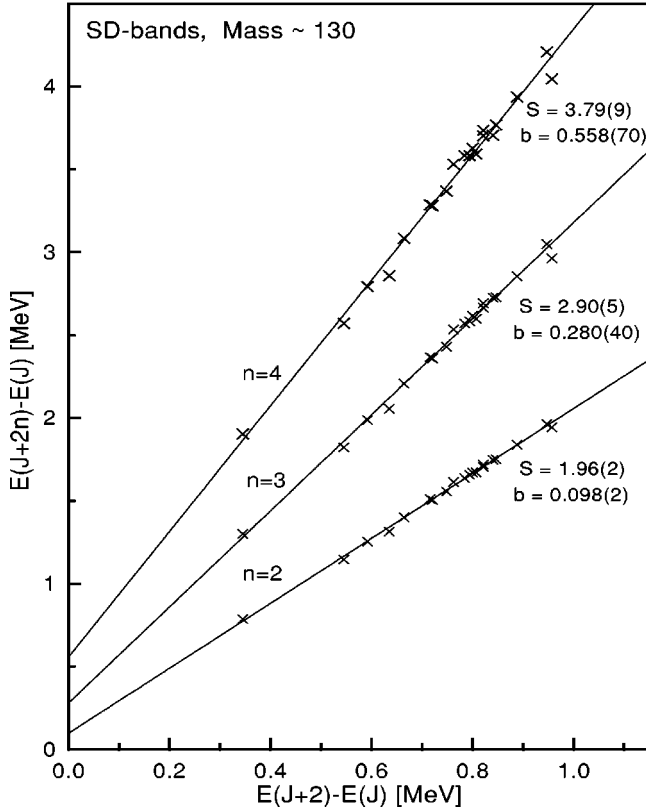
FIG. 18. Energy correlation plots for the first states in the SD bands of the $A = 130$ mass region, and their straight line fits.
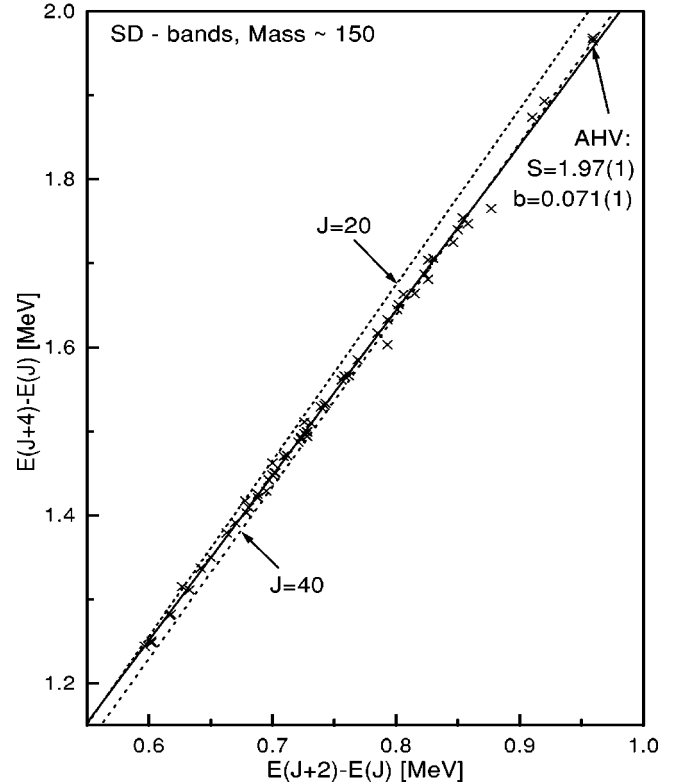

FIG. 19. Energy correlation plots for the lowest states in the SD bands from the $A = 150$ mass region. The full line is the ''AHV'' fit [Eq. (13)] to the data, while the dotted lines represent Eq. (12) for spins $J = 20$ and 40, respectively.

The behavior is again quite close to that of Eq. (13), with a rather small scatter of the points; the slight increase of the deviation of the slopes of the fitted lines from the AHV values (2.0,3.0,4.0, . . .) for higher n values may reflect a slight change of the moment of inertia with increasing spin.

As is well known, for most of the SD bands, the links to the lower, normally-deformed states have not been found and therefore their spin values are known only approximately. Some indication of the spin values can be obtained by examining the type of plots discussed until now and their intersection with the lines defined by Eq. (12). Figure 19 shows such a comparison for the SD bands from the $A \approx 150$ mass region. This plot shows that the spin values of the lowest states of these bands are between 20 and about 40, which agrees with other methods to estimate tentative assignments [14]. However, spin assignments more precise than a few units are difficult to make due to the small differences between the slopes of the lines given by Eq. (12) for small spin differences. It is also difficult to say whether the experimental data cluster around points representing different spins, as discussed above.

B. Phase transitions

In the case of even-even nuclei, the transition between the ''AHV regime'' (which characterizes the large class of nuclei with $R_{4/2}$ between 2.05 and 3.15, Fig. 1) and the ''rota-

tional'' regime (nuclei with $R_{4/2} > 3.15$, Fig. 4) has been studied in [1]. The essential aspect of this transition is shown in Fig. 20: as indicated by the empirical derivative $dE(4_1^+)/dE(2_1^+)$ it is very rapid, as it takes place in a very narrow region of $E(2_1^+)$ values around a *critical* value $E_c \approx 125$ keV. It was argued in Ref. [1] that this transition presents all the features of a *critical phase transition*, while in Ref. [15] further support was given by examining the behavior of other quantities. The question of phase transitional behavior in finite nuclei has been further addressed from a more general standpoint in Ref. [16]. Here we wish to consider the situation in odd-A nuclei.

As shown by the experimental data discussed in previous sections, in both odd-A and odd-odd nuclei the same two regimes are also evidenced. However, it is more difficult to study the transition between them since they are, formally, very similar [both are described by the ''AHV'' formula (13), the only difference being the different value of ε_4: about 150 keV for the nonrotational nuclei, and about 95 keV for the rotational ones]. Recall that the rotational bands studied do not in general follow the expected rotational formula Eq. (12). To disentangle the characteristics of the transition between the two regimes in this case, it is better to follow a well defined structure which is found in both. A good example is in the $\nu i_{13/2}$ bands of the isotopes of Er, Yb, Hf, and W [5,17]. The evolution of the lowest energy levels
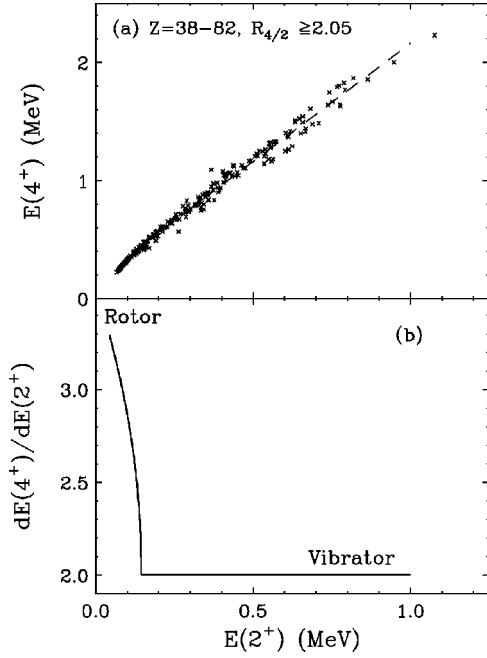
FIG. 20. (a) Correlation of $E(4_1^+)$ with $E(2_1^+)$ for all collective nuclei $(R_{4/2} \geqslant 2.05)$ for $Z=38-82$. (b) The derivative $dE(4_1^+)/dE(2_1^+)$ against $E(2_1^+)$ obtained from the fit of data in part (a) (see Ref. [1]).

within this structure, starting from the state with spin $J = 13/2$, is shown in Fig. 21. In the lower part of this figure one can see that in all these isotopic chains the lowest mass isotopes belong to the AHV regime. By increasing the mass number one moves first downwards along the AHV line, with a slope 2.0 to a point where the curve turns rapidly and moves towards the rotational limit (the line of slope 2.25, corresponding to $J=13/2$). The transition is fairly rapid—it takes place in a rather narrow range of $E(1)$ values near a critical value, $E_t \approx 210$ keV, which we call the ''turning point'' [5,17]. The derivative of a smooth curve drawn through the trajectory of the data points, $dE(2)/dE(1)$, is discontinuous at the value $E(1)=E_t$, as it has two branches which at E_t go to plus and minus infinity, respectively (for this reason, this behavior was called an ''inverted λ-anomaly'' in Ref. [17]).

The upper part of Fig. 21 shows a plot of $E(1)$ for the odd-A nuclei against $E(1)$ for the even-even core, that is $E(17/2)-E(13/2)$ against $E(2_1^+)$. The figure shows that the turning point, which is the ''critical'' point of this transition, occurs at the same 2_1^+ energy of the even even core which is the critical point (see Figs. 1 or 20) for that class of nuclei. That is, the variation of $E(1)$ in odd-A nuclei against the $E(2_1^+)$ energy in the core shows a minimum at the E_t value, which corresponds to the value $E(2_1^+)=E_c$. One can qualitatively explain the change of structure that takes place around E_t. At energies of $E(2_1^+)$ larger than E_c, the deformation is small and the odd particle is either weakly coupled or decoupled, therefore the $E(1)$ energy in the odd-A nucleus closely follows the variation of $E(2_1^+)$ as seen in the upper part of Fig. 21. At the value $E(2_1^+) \approx E_c$, the rota-
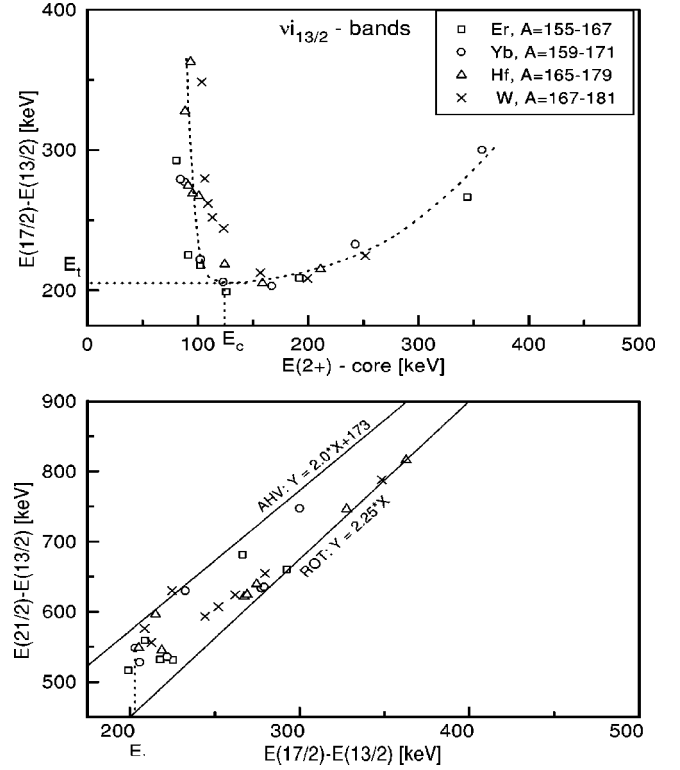

FIG. 21. Illustration for the transition between nonrotor (AHV-type) and rotor odd-A nuclei. The data represent the $\nu i_{13/2}$ bands in the indicated nuclei, and the excitation energies are taken relative to the $13/2^+$ state. In the lower part of the figure, for each isotopic chain, beginning with the lighter mass, one moves downwards along the AHV line to the turning point E_t (at about 210 keV) where the curve rapidly changes the sense and approaches the rotational limit. The upper part shows that the turning point in the odd-A nuclei corresponds to the critical point E_c (about 125 keV) from the even-even core nuclei [1].

tional regime settles quickly in for the core nuclei, and this change forces a change towards the strong coupling regime in the odd-mass nuclei. Although the $E(2_1^+)$ energy in the cores continues to decrease, the $E(1)$ energy in the strongly coupled band starts to increase towards the strong coupling limit $E(1)=32(\hbar^2/2\mathcal{I})$ [Eq. (11)] which is much larger than the value $E(2_1^+)=6(\hbar^2/2\mathcal{I})$ in the core. Thus, it is clear that the AHV to rotor transition in the odd-A nuclei is intimately connected with the critical phase transition from the even-even nuclei.

C. Unified formula for quasiband energies

The empirical data presented in Sec. II and discussed above provide rich evidence for the fact that a large variety of quasibands in all classes of collective nuclei are, surprisingly, well described by the AHV expression, Eq. (2) with *constant* anharmonicity ε_4. This statement even applies to deformed odd-A rotational nuclei. The only exception is deformed even-even rotational nuclei which follow the rotor formulas [i.e., Eq. (2) with *variable* $\varepsilon_4=8\hbar^2/2\mathcal{I}$]. Although the meaning of the AHV behavior is different for the nonrotational and rotational nuclei, an important, practical aspect
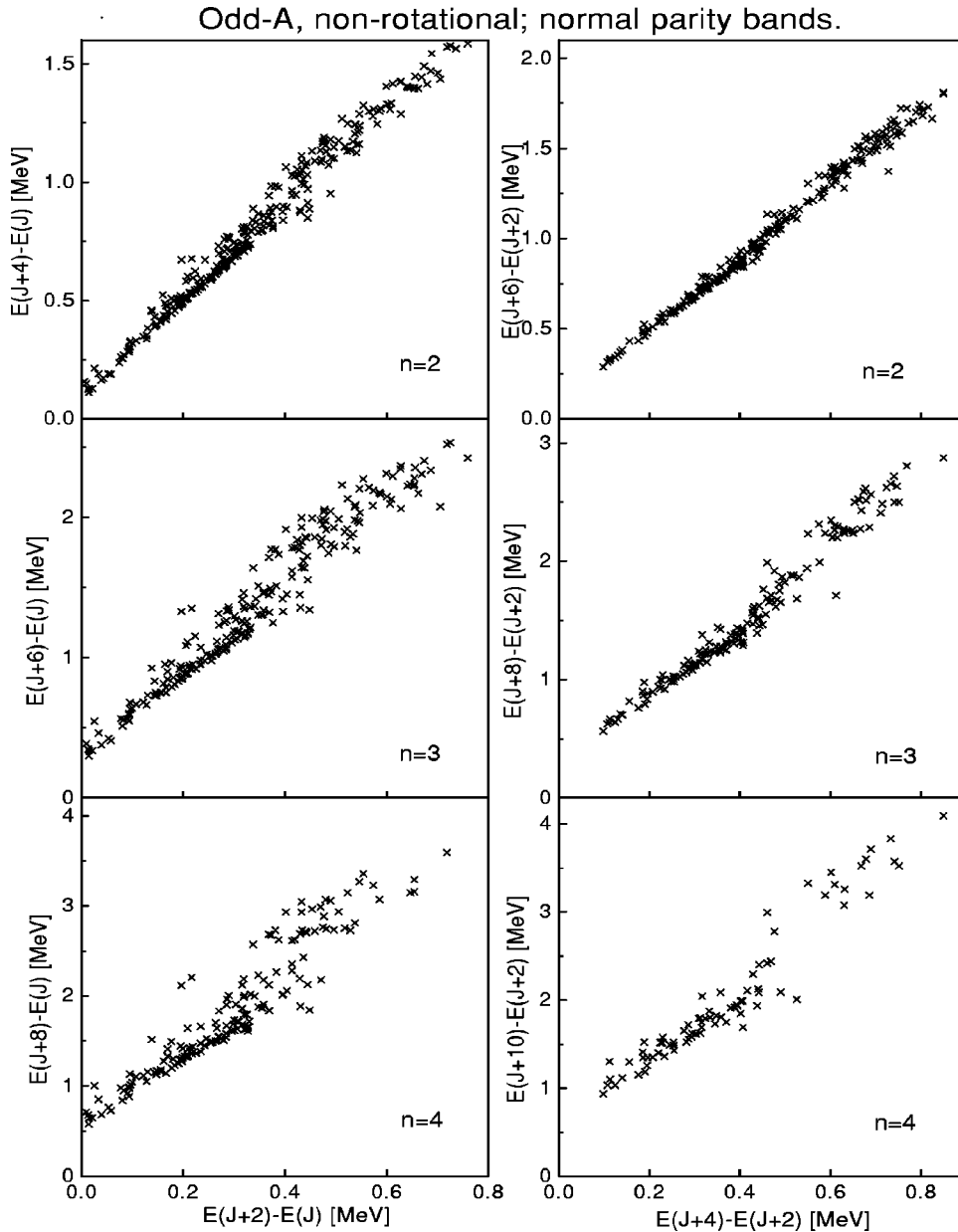
Odd-A, non-rotational; normal parity bands.

FIG. 22. Illustration of the scatter of the points in energy correlation plots. The experimental data are the same with those in Fig. 5. In the left hand panels the reference state is the lowest state from the band (of spin J), whereas in the right hand panels it is the second state (of spin $J+2$).

is that almost all quasiband structures in collective nuclei can be described analytically with the same formula.

We have placed the emphasis, until now, on the lowest states of the bands [Eq. (2) was verified, usually, up to $n=3$ or 4]. We now extend the study to higher states as well; for this purpose each band has been followed up to the highest known spin, or up to the crossing with another band (upbending or backbending). A common feature of the empirical AHV correlations is the increase of the scatter of the points around the average AHV behavior as one moves upwards in the band. This is illustrated in Fig. 22 for normal parity bands in odd-A nonrotational nuclei with $Z=32-80$. The data show the best AHV correlation for the first two energies in the band [$n=2$ in Eq. (2)]; the AHV correlation persists reasonably well for the third excitation energy ($n=3$), but, usually, with more scatter of the points, and the scatter increases continuously for the higher states. The increasing scatter does *not* mean, however, that the AHV cor-

relation gradually disappears. One finds again a nice AHV correlation if one starts from *any other higher state of the band* which is taken as origin (or ''zero-phonon'' state). This is also illustrated in Fig. 22 (right-hand panels). Thus, it is clear not only are quasiband energies well represented by the AHV formula, but, further, that the deviations of the points corresponding to different n values from the mean AHV behavior are highly correlated.

These correlations can be unraveled by studying relationships between the experimental excitation energies of more than three successive states from the band, for all collective even-even and odd-A nuclei [6]. If we denote by $E_\gamma(n)$ the ''transition energy'' from the state n of the band to the state below it, $n-1$: $E_\gamma(n)=E(n)-E(n-1)$, the basic observation is that, for all the bands investigated, we have, with a reasonable accuracy, for any n,
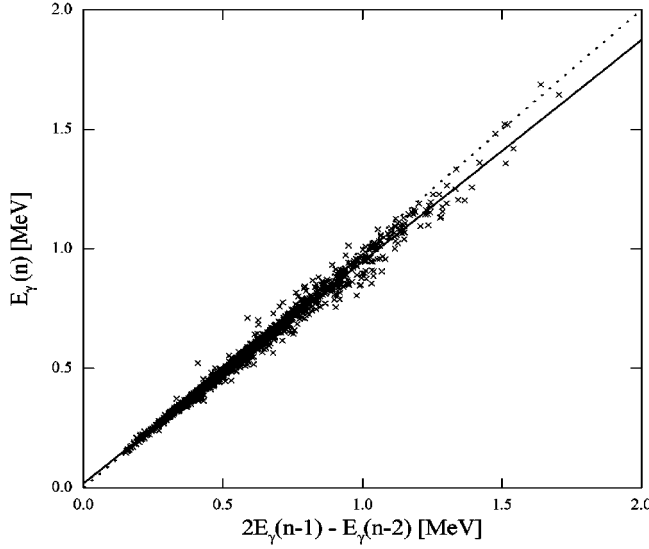
$$E_\gamma(n)=2E_\gamma(n-1)-E_\gamma(n-2). \qquad (17)$$

FIG. 23. Correlation between band ''transition'' energies—this plot shows the two quantities which appear in the left and right side of Eq. (17), respectively. The data are those for both rotational and nonrotational even-even and odd-A nuclei. A band with n known transitions contributes $n-2$ points to this plot. There are about 750 bands with at least three known transitions, and one band goes up to $n=9$. The dotted line represents Eq. (17), whereas the full line is the fit with Eq. (18) with $c_1=0.93$ and $c_2=19$ keV.

This is, in fact, an exact prediction of both the AHV equation (2) and of the rotational formula (10). Figure 23 shows the correlation between $E_\gamma(n)$ and $2E_\gamma(n-1)-E_\gamma(n-2)$ for about 750 bands for which at least three successive transitions are known (yrast bands of rotational even-even nuclei are also included). As observed in this figure, the large number of points (about 2000) are very well grouped into a compact pattern which deviates only slightly from Eq. (17). This correlation is actually even better approximated by a more general equation:

$$E_\gamma(n)=c_1[2E_\gamma(n-1)-E_\gamma(n-2)]+c_2, \qquad (18)$$

where c_1 and c_2 are two parameters. This new formula can be rewritten in terms of excitation energies as

$$E(n)=E(n-1)+c_1[2E(n-1)-3E(n-2)+E(n-3)]$$
$$+c_2. \qquad (19)$$

This is a recurrence formula which gives the energy of any state in the band as a function of the energies of the three states below it—the whole band can therefore be calculated by starting from the experimental $E(1)$ and $E(2)$ values, using some adequate values for the parameters c_1 and c_2 [the energy $E(0)$ of the ''basis'' state can be chosen as zero]. In Ref. [6], least squares fits have been performed for different sets of bands/nuclei, using formula (19), and values of the parameters c_1 and c_2 have been determined. It was found that a rather good description can be obtained for a large number of bands, up to the highest known state, with the same values c_1,c_2. In general, c_1 was found close to 1.0 (between 0.92 and 0.98)—as visible in Fig. 23, and c_2 from

a few keV to about 20 keV. Formula (19) was found more accurate for rotational nuclei (for which c_1 is closer to 1.0).

The recurrence relation (19) can be used also to give a generalization of the AHV expression of Eq. (2) in the *approximation* $c_1=1$. In this case one gets, explicitly,

$$E(n)=nE(1)+\frac{n(n-1)}{2}\varepsilon_4+\frac{n(n-1)(n-2)}{6}\varepsilon_6, \qquad (20)$$

with $\varepsilon_4=E(2)-2E(1)$ and $\varepsilon_6=2c_2$. This is a second order AHV expression, a generalization of Eq. (2) which, in addition to ε_4, has another anharmonicity, ε_6. The result is not new: in Ref. [18] it was proposed that this next order generalization of Eq. (2) is one of the best formulas to describe the yrast bands of both the ''AHV'' and rotor even-even nuclei. However, Eq. (20) now has a sounder basis: it is derived from the compact correlation of many experimental data (Fig. 23), and, moreover, Eq. (20) is now seen as an approximation to a more general formula, Eq. (19).

Since Eq. (19) provides, as a limit, the second order AHV formula (20), we call the recurrence formula (19) a ''*generalized anharmonic vibrator*'' (GAHV). With it *all* band structures in both rotational and nonrotational nuclei (even-even, odd-A and odd-odd) are well described by a single expression, the GAHV formula (19). A good approximation of this formula is Eq. (20); the lowest order AHV correlations discussed at length in this article are a reflection of this more general formula, and it is seen now that the increased scatter of the points with respect to Eq. (2), illustrated by Fig. 22, reflects the need for an additional higher order anharmonicity. Equations (19) or (20) can be applied to any band, up to the highest spin, with excellent results, if $E(1)$, ε_4 and ε_6 are considered free parameters and are fitted to the data. An attractive aspect of the present results is, however, that Eq. (19) describes reasonably well large sets of bands (or nuclei), with *fixed* c_1,c_2 values.

The study of Ref. [6] was restricted to the yrast bands in the even-even nuclei, and the 1qp bands in the odd-A nuclei, but obviously can be generalized to all the other bands added in the present work, which have been found in equally good agreement with the first order AHV expression (2). One can speculate, although no attempts were made to look at other excited band structures (such as 2qp bands in even-even nuclei, 3qp bands in odd-A nuclei, etc.), that the GAHV formula (19) describes well *any band structure* that is not perturbed by a band crossing. The collective band structures in nuclei thus reveal a universal phenomenology.

IV. THEORETICAL CALCULATIONS

The nearly universal anharmonic vibrator behavior of the lowest quasiband structures in all collective nuclei is a real challenge for nucler structure theories. Analytical formulas which appear to describe well both the rotational and nonrotational structures remain empirical findings. Microscopic model approaches aiming at unraveling the factors that determine such a universal phenomenology have not been made so far. On the other hand, insight into the empirical
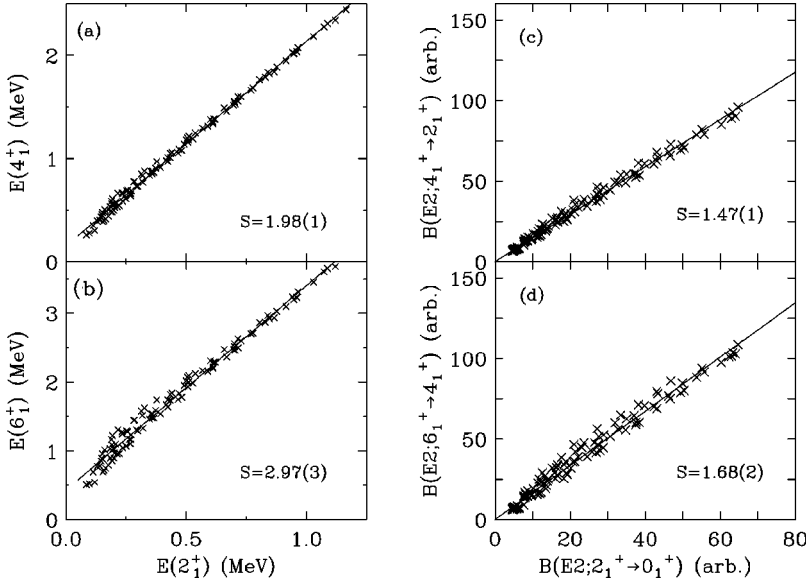
FIG. 24. IBA calculations with $\kappa = 0.03$ MeV for a wide mesh of ϵ, χ, and N_B values that give $R_{4/2} = 2.05$–3.15. (a) Correlation of $E(4_1^+)$ with $E(2_1^+)$. (b) Correlation of $E(6_1^+)$ with $E(2_1^+)$. (c) Correlation of $B(E2;4_1^+ \rightarrow 2_1^+)$ with $B(E2;2_1^+ \rightarrow 0_1^+)$. (d) Correlation of $B(E2;6_1^+ \rightarrow 4_1^+)$ with $B(E2;2_1^+ \rightarrow 0_1^+)$.

phenomena can be gained by using phenomenological models which have been successfully applied to real nuclei. In this section we summarize existing interacting boson approximation (IBA) model calculations and present new results with the geometrical collective model (GCM).

A. The interacting boson and interacting boson-fermion model

The IBA model [19] for even-even nuclei is a rather natural choice to investigate the predicted energy correlations. The IBA model embodies the well-known collective limits (vibrational, γ-soft and rotational) as well as the different transitions between them. It spans this variety of structures with a small number of parameters. In the same way, the interacting boson-fermion approximation (IBFA) model [20], in which a particle is coupled to an IBA core, covers the large variety of coupling schemes met in odd-A nuclei.

In Ref. [2], IBA calculations were made with an extended consistent-Q formalism (ECQF) Hamiltonian [21,22]:

$$H = \varepsilon \hat{n}_d - \kappa \hat{Q} \hat{Q}, \tag{21}$$

with

$$\hat{Q} = (s^\dagger \tilde{d} + d^\dagger s) + \chi (d^\dagger \tilde{d})^{(2)},$$

which spans the full variety of collective modes in terms of only three parameters, ε, κ, and χ. Each nucleus is characterized by a boson number N_B given by half the total number of valence particles or holes. We performed a mesh of calculations, covering all areas of the symmetry triangle. In these calculations, κ was kept constant at a value that determines the height (or intercept) of the energy correlation trajectories in even-even nuclei, namely $\kappa = 0.032 \pm 0.002$ MeV [2]. N_B, ϵ, and χ were varied in a three-dimensional mesh through the ranges $4 \leq N_B \leq 16$, $0 \leq \epsilon \leq 1.25$ MeV, and $0 \leq |\chi| \leq \sqrt{7}/2$. The only condition was that the $R_{4/2}$ values covered the same range as those in Fig. 1(a), namely $2.05 \leq R_{4/2} \leq 3.15$. Figure 24 shows the results of the IBA calculations [2] of the yrast states in nonrotational

even-even nuclei. They reproduce the main features of the empirical data almost exactly [compare with Fig. 1(a)].

In calculations for odd-A nuclei done in Ref. [5], the Hamiltonian also contains additional terms representing single fermion energies and the interactions of the odd fermion with the boson core. In the general case, where the fermion can occupy any of several shell model orbits, the number of parameters increases very rapidly and the model becomes difficult to use in practice without some simplification schemes. For a single-j orbit, however, such as the UPO case, the situation simplifies dramatically. In such a case, the IBFA Hamiltonian contains, in addition to the ECQF Hamiltonian (21), and a single fermion energy, a standard quadrupole-quadrupole and an exchange boson-fermion interaction which are characterized by only two strength parameters, Γ_0 and Λ_0, respectively. The calculations [5] used the same range of N_B, ϵ, and χ values as for the even-even case. The particle-core interaction parameters took on the following ranges: $-3.0 \leq \Gamma_0$ (MeV) ≤ 3.0 and $0 \leq \Lambda_0$ (MeV) ≤ 6.0. (The scale factor v_j^2 was set at 0.25.) A random number generator was used to arbitrarily select values for the five quantities N_B, ϵ, χ, Γ_0, and Λ_0. Any choice for the core parameters N_B, ϵ, and χ that corresponds to transitional nuclei, namely $2.05 \leq R_{4/2} \leq 3.15$, was then used. In all, about 500 calculations were performed. The results are compared with the data (for two unique parity orbits, $1g_{9/2}$ and $1i_{13/2}$) in Fig. 25. Again, the calculations reproduce the main features of the experimental data—not only the linear patterns, but also the characteristic scatter of the points are reproduced.

The implications of this good description of the experimental correlations by the IB(F)A model calculations are rather profound. Once an appropriate κ value is chosen to reproduce some point on the empirical correlation plot, the IBA (or IBFA) model automatically reproduces the trend of the data. The calculated points correspond to a few hundred randomly assorted values of N_B, ε, χ (with Γ_0, Λ_0, and v_j^2, the shell occupancy, added for the odd-A nuclei). The key

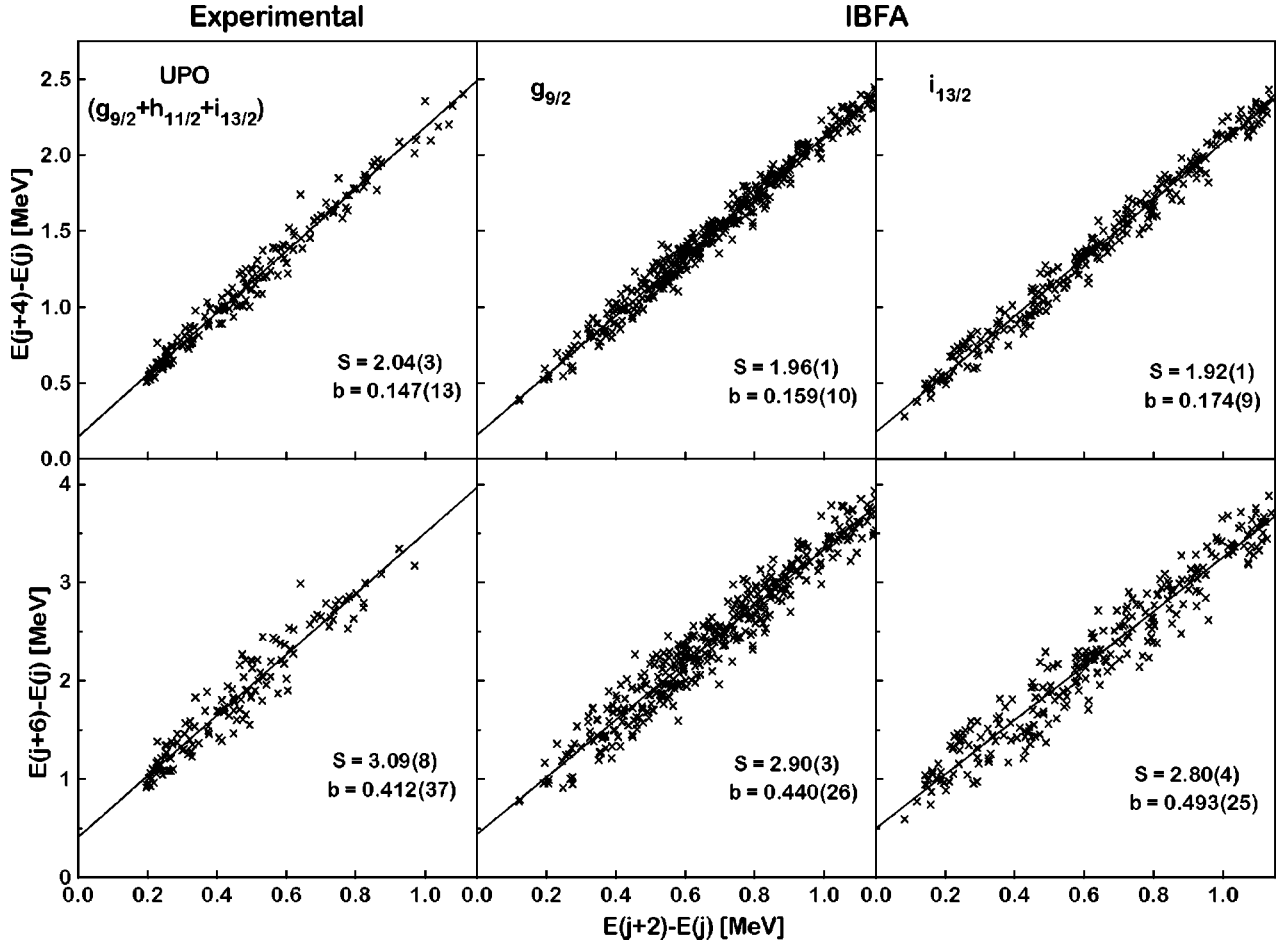**Experimental**   **IBFA**

FIG. 25. Comparison between experimental data and IBFA model predictions. Experimental data are those for unique parity quasibands in nonrotational odd-A nuclei. All data available for the orbitals $g_{9/2}$, $h_{11/2}$, and $i_{13/2}$ are contained in this plot, and the reference state is always taken to be that of spin j (the spin of the UPO). On the right are the results of several hundred IBFA model calculations, with randomly chosen parameters, as described in the text and Ref. [5]. In these calculations, one single orbital was coupled to the IBA core, either $g_{9/2}$ or $i_{13/2}$, as indicated. The curves are straight line fits, and give the slopes S and the intercepts b as indicated.

point is that *no attempt* whatsoever is made to ''fit'' the data. If the data were different, (e.g., had a different slope), the IB(F)A models would have not been able to reproduce them (unless κ were fitted separately for each nucleus). Thus, we are dealing here with a fundamental, and robust, prediction of the IBA (IBFA) model. These theoretical results are not yet fully understood, although the IBA calculations can be reproduced in an approximate analytical way [24].

B. The geometric collective model

Striking as these results are, it is not known whether such linear correlations are a feature special to the IBA or whether other collective models, based on different points of view, also give similar behavior. Understanding this point could, for example, give some guidance as to whether the correlations will hold up in exotic nuclei far from stability.

To test whether other models also give a slope of 2 in an $E(4_1^+)-E(2_1^+)$ correlation plot, we have carried out extensive sets of calculations with the geometric collective model (GCM) [25]. We use a recently developed approach [26] in which the Hamiltonian of Ref. [25] is simplified to the following form:

$$H = T + V, \tag{22}$$

where

$$T = \frac{1}{B_2}[\hat{\pi} \times \hat{\pi}]^{(0)} \tag{23}$$

and

$$V = C_2'\beta^2 + C_4'\beta^4 - C_3'\beta\cos^3(3\gamma), \tag{24}$$

where C_2', C_3', C_4' are parameters similar to C_2, C_3, and C_4 of Ref. [25] except that they absorb awkward numerical constants. With this Hamiltonian a harmonic vibrator spectrum is obtained if $C_4' = C_3' = 0$ and C_2' is positive. A deformed rotor is given if $C_2' < 0, C_4', C_3' > 0$. This gives a potential with a deformed minimum in β and a γ-dependence with a minimum at $\gamma = 0°$ and a slope related to C_3'. A γ-unstable deformed nucleus is similar to the rotor but with $C_3' = 0$. Thus, the GCM leads to a symmetry or structural triangle [26] similar to that developed [23] for the IBA.
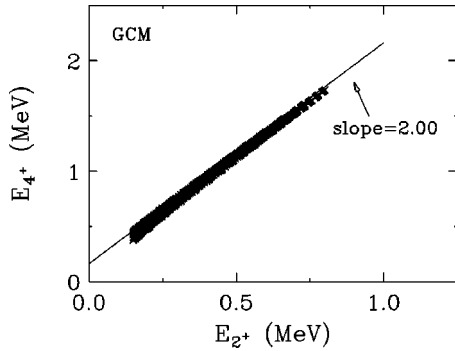
FIG. 26. Correlation of $E(4_1^+)$ with $E(2_1^+)$ for nonrotational nuclei [$R_{4/2}<3.15$ and $E(2_1^+)>0.15$ MeV] for a wide mesh of GCM calculations with $C_2'=-100$ to -350 MeV, $C_3'=0$ to 100 MeV, and $C_4'=0$ to 4000 MeV.

With the Hamiltonian of equations (22)–(24), a full mesh of calculations covering the parameter ranges $C_2'=-100$ to -350 MeV, $C_3'=0$ to 100 MeV, and $C_4'=0$ to 4000 MeV was carried out. These ranges cover the structures in most of the structural triangle discussed in Ref. [26]. The mass parameter, B_2, was set at 100×10^{-42} MeV s^2, but this choice only affects the scale of the calculated energies. All calculations that gave $R_{4/2}<3.15$ and $E(2_1^+)>0.15$ MeV (i.e., all calculations which gave nonrotational nuclei) are shown in Fig. 26. They are striking. Like the IBA, the GCM *also* reproduces the empirical correlations almost exactly; the slope is almost identically 2.0. The intercept is controlled by the parameter C_2', analogous to the dependence on κ in the IBA. The arbitrary parameter combinations, included in the GCM calculations, imply, as with the IB(F)A, that these results are highly robust and that, were the data different, the GCM could not readily reproduce them.

V. CONCLUSIONS

To summarize, we have shown that the linear correlations of yrast energies originally discovered in even-even non-rotational nuclei, and subsequently shown to exist in odd-A nuclei as well, *also apply* to excited intrinsic states (e.g., $K=0^+$ bands, γ bands, superdeformed bands), and to odd-odd nuclei. Furthermore, we have studied the GCM model and shown that, like the IBA, it reproduces these correlations extraordinarily well and robustly, that it does so for virtually arbitrary combinations of parameters, and that for it to do otherwise would be difficult or impossible.

All these results once again point to and reinforce the AHV interpretation of these quasiband states.

One particularly intriguing discovery is that bands in *deformed* nuclei follow the AHV expression *rather* than the usual rotational formula. For $K=1/2$ bands, this behavior can be understood as a consequence of the Coriolis interaction but it is not understood for other bands. If it results from a second order Coriolis mixing effect, there remains no simple understanding of why such effects are so systematic and why they always lead back to the AHV expression.

Finally, it was shown that a single analytic expression, which is in essence a generalized anharmonic vibrator (generalized in the sense that it contains higher order anharmonicities) is capable of describing *any* type of quasiband structure. But *why* the AHV works so well, for such varied states, in such disparate nuclei, always with an almost *constant* anharmonicity, and why quite different model approaches are themselves virtually locked into the same results—in a robust way—is still unknown and, in our view, is a significant challenge both to extend this work by studying other empirical correlations and to investigate the predictions of microscopic theories based on effective nucleon-nucleon interactions.

[1] R. F. Casten, N. V. Zamfir, and D. S. Brenner, Phys. Rev. Lett. **71**, 227 (1993).

[2] N. V. Zamfir and R. F. Casten, Phys. Lett. B **341**, 1 (1994).

[3] N. V. Zamfir, R. F. Casten, and D. S. Brenner, Phys. Rev. Lett. **72**, 3480 (1994).

[4] D. Bucurescu, G. Căta-Danil, M. Ivaşcu, L. Stroe, and C. A. Ur, Phys. Rev. C **49**, R1759 (1994).

[5] D. Bucurescu, N. Mărginean, I. Căta-Danil, M. Ivaşcu, L. Stroe, and C. A. Ur, Phys. Lett. B **386**, 12 (1996).

[6] D. Bucurescu and N. Mărginean, Phys. Rev. Lett. **79**, 31 (1997).

[7] D. Bucurescu, N. V. Zamfir, G. Căta-Danil, M. Ivaşcu, L. Stroe, C. A. Ur, and R. F. Casten, Phys. Lett. B **376**, 1 (1996).

[8] Quasiband structures for all even-even nuclei considered in this work are from Nuclear Data Sheets through June 1998 and those for odd-A and odd-odd nuclei were extracted from the Evaluated Nuclear Structure Data File (ENSDF), maintained by the National Nuclear Data Center, Brookhaven National Laboratory.

[9] D. M. Brink, A. F. R. de Toledo Piza, and A. K. Kerman, Phys. Lett. **19**, 413 (1965).

[10] T. K. Das, R. M. Dreizler, and A. Klein, Phys. Rev. C **2**, 632 (1970).

[11] C. A. Mallmann, Phys. Rev. Lett. **2**, 507 (1959).

[12] H. Ejiri, M. Ishihara, M. Sakai, K. Katori, and T. Inamura, J. Phys. Soc. Jpn. **24**, 1189 (1968).

[13] W. T. Chou, R. F. Casten, N. V. Zamfir, D. S. Brenner, and D. Bucurescu, Nucl. Phys. **A580**, 33 (1994).

[14] B. Singh, R. B. Firestone, and S. Y. Frank Chu, Nucl. Data Sheets **78**, 1 (1996).

[15] A. Wolf, R. F. Casten, N. V. Zamfir, and D. S. Brenner, Phys. Rev. C **49**, 802 (1994).

[16] R. F. Casten, Dimitri Kuznezov, and N. V. Zamfir, Phys. Rev. Lett. **82**, 5000 (1999).

[17] D. Bucurescu, G. Căta-Danil, M. Ivaşcu, L. Stroe, and C. A. Ur, in *Perspectives of the Interacting Boson Model*, edited by R. F. Casten *et al.* (World Scientific, Singapore, 1994), p. 389.

[18] N. V. Zamfir and R. F. Casten, Phys. Rev. Lett. **75**, 1280 (1995).

[19] A. Arima and F. Iachello, Phys. Rev. Lett. **35**, 1069 (1975).

[20] F. Iachello and O. Scholten, Phys. Rev. Lett. **43**, 679 (1979).

[21] D. D. Warner and R. F. Casten, Phys. Rev. Lett. **48**, 1385 (1982).

[22] P. O. Lipas, P. Toivonen, and D. D. Warner, Phys. Lett. **155B**, 295 (1985).

[23] R. F. Casten and D. D. Warner, Rev. Mod. Phys. **60**, 389 (1988).

[24] R. V. Jolos, P. von Brentano, R. F. Casten, and N. V. Zamfir, Phys. Rev. C **51**, R2298 (1995).

[25] G. Gneuss and W. Greiner, Nucl. Phys. **A171**, 449 (1971).

[26] Jing ye Zhang, R. F. Casten, and N. V. Zamfir, Phys. Lett. B **407**, 201 (1997).